PASSIVE MULTIPLE BEAM COMBINATION IN OPTICAL FIBERS
VIA STIMULATED BRILLOUIN SCATTERING

THESIS

Kirk C. Brown, Captain, USAF

AFIT/GAP/ENP/06-01

AFIT/GAP/ENP/06-01

Passive multiple beam combination in optical fibers
via Stimulated Brillouin Scattering

THESIS

Presented to the Faculty

Department of Engineering Physics

Graduate School of Engineering and Management

Air Force Institute of Technology

Air University

Air Education and Training Command

In Partial Fulfillment of the Requirements for the

Degree of Master of Science (Applied Physics)

Kirk C. Brown, B.S.

Captain, USAF

March 2006

AFIT/GAP/ENP/06-01

Passive multiple beam combination in optical fibers
via Stimulated Brillouin Scattering

Kirk C. Brown, B.S.

Captain, USAF

Approved:

/signed/   06 Mar 2006
——————————————————————   ——————————————————
Timothy H. Russell (Chairman)   date

/signed/   06 Mar 2006
——————————————————————   ——————————————————
Thomas G. Alley (Member)   date

/signed/   06 Mar 2006
——————————————————————   ——————————————————
Matthew J. Bohn (Member)   date

AFIT/GAP/ENP/06-01

Abstract

Many active methods of scaling laser brightness have been demonstrated in recent years. The goal of this research was to demonstrate the feasibility of passively combining multiple laser beams using Stimulated Brillouin Scattering (SBS) in a long multimode optical fiber. This method of combination employed a "Gatling gun" fiber array that allowed several collimated beams to be focused by a lens into an optical fiber. The retroreflected Stokes beam is passed through the center of the beam combiner for analysis. In addition to experimental methodology and equipment used, the theoretical and historical background of SBS in optical fibers is provided.

The ability to combine four single-mode off-axis input beams using a fiber array and a long multimode optical fiber was demonstrated. The Stokes beam generated by the four off-axis input beams was found to be near Gaussian with an M^2 value of ≤ 1.08. The reflected Stokes beam intensity was erratic with no discernible period. The maximum average reflected power was approximately 50 mW with a conversion efficiency of 3.5% and a slope efficiency of 11.4%. The peak reflected power was measured to be over 400 mW with a conversion efficiency of 42%. The threshold required to generate SBS in this configuration was quadruple the predicted power required to generate SBS using an on-axis pump beam.

The deleterious effects of the addition of an off-axis side channel was demonstrated. When a Stokes beam was created using an on-axis pump beam, the result was a stable Stokes beam. The addition of just one side channel caused the Stokes beam to become erratic and fluctuate in intensity with no discernible period. A hypothesis is provided and compared to current theory. The success of this thesis suggests the possibility of a new approach to pumping a fiber Brillouin laser which could reduce the threshold, increase conversion efficiency, and maintain excellent beam quality.

Acknowledgements

First and foremost I thank God for allowing us the ability to use our intelligence to describe the workings of nature and derive pleasure and utility from doing so. I want to thank the Air Force and the taxpayers for allowing me an opportunity to perform basic research and be paid for it. Dr. Won Roh, LtCol Tom Alley, and Maj Tim Russell were instrumental in teaching me all I know about lasers and lab work even though I did not get some of it the first time around. I want to thank Lt Brian Flusche, Capt Brent Grime, and Capt Nate Terry for showing me many indispensable lab tricks and techniques. And of course I cannot forget my mother who always took me to the library to check out piles of science books despite her predictions of widespread disaster and public panic during my model rocket launches. Most of all, I thank my wife for her constant source of sunshine when all I saw were dark clouds. Without her I would not be where I am today. This is for her.

Kirk C. Brown

Table of Contents

List of Figures

List of Tables

Passive multiple beam combination in optical fibers via Stimulated Brillouin Scattering

I. Introduction

SINCE the invention of the laser, many have looked for a way to combine the coherent output from many low power sources and efficiently scale power. By using many low power modular sources, one can reduce costs, size, and cooling requirements yet maintain high power and excellent beam quality. Currently, the most common method for achieving high powers is to build large monolithic lasers. For materials processing work, such as heavy duty cutting or welding, chemical and solid state lasers are still the most cost effective and mature technology. However, these lasers are large, expensive, and require active cooling systems. For defense applications that require up to 1 MW of continuous power, the only technology that can reach this power level are chemical lasers such as Hydrogen-Flourine (HF) and the Chemical Oxygen Iodine Laser (COIL) used onboard the Airborne Laser (ABL). However, high power chemical lasers suffer from logistical complications, large size, and limited magazine depth, making tactical operation impossible with current technology.

Semiconductor laser diode arrays (LDAs) attack the problem of high power by employing many low power modules in a two-dimensional array. In recent years, this method has been used to achieve continuous wave (CW) output powers in the kilowatt range. In the materials processing industry, LDAs have begun to replace the older solid state and chemical systems. LDAs offer customers long lifetimes, energy cost savings, and reduced floor space requirements over traditional chemical or solid state systems. But diode lasers are not the panacea once thought. Since the gain region and aperture of diode lasers are small, the output from individual elements of an array suffers from beam spreading and astigmatism. By tuning the coherence of individual element members, adjusting the duty cycle of the array, and using complicated optics, beam

quality can be quite good. However, to maintain their high efficiency, LDAs require an effective cooling system to keep the semiconductor junctions at optimum temperature. These cooling systems are complex and significantly increase the logistical footprint of the LDA. Further, large cooling systems are heavy and themselves inefficient, which makes tactical defense applications difficult to implement.

Even if an array of low power, high efficiency lasers were developed, the problem of combining the outputs into a coherent, well formed beam must still be solved. For two beams to combine, they must spatially coherent. In a two-dimensional array, spatial incoherence will result in a diffraction pattern that does not permit all of the energy to be concentrated into one lobe. For the beams to be spatially coherent, the phase of each element in an array must be precisely tuned. In the last few years, several methods have shown the ability to phase lock the entire array, but these methods required active techniques or optical components. A passive solution of combining multiple beams into one coherent beam would be ideal, since no electromechanical control would be required.

For the past few decades, stimulated Brillouin scattering (SBS) in optical fibers has been vigorously investigated in optical fibers. While SBS is viewed by the telecommunications industry as a deleterious effect that requires complex methods to reduce the retroreflected light to acceptable levels, the military has found a potential solution to the problem of coherently combining multiple beams. SBS has been used successfully in the past to combine and clean up an aberrated beam [7]. At AFIT, research conducted in the last few years has been successful combining two beams from mutually incoherent sources [13]. Recently it has been demonstrated that the output from two fiber amplifiers can be successfully phased and combined using SBS. [8] The task remains to efficiently combine more than two beams.

Chapter II of this thesis will provide the reader sufficient review of fiber optics and stimulated Brillouin scattering. Chapter III will detail the methods and equipment used to investigate beam combination and cleanup. Chapter IV will present the

results and analysis of the data collected, and Chapter V will provide a brief review of the progress made and suggestions for further research.

II. Theoretical Background

CHAPTER II provides the reader a refresher in basic optical waveguide theory and also provides an introduction to Stimulated Brillouin Scattering. The experimental work and analysis in this thesis rely on nonlinear effects and propagation of electromagnetic waves in optical fibers. A brief historical review of SBS in optical fibers will be given in Section 2.3

2.1 Propagation of Light in Optical Fibers

Since ancient times, mankind has struggled to comprehend the nature of light. With the success of quantum theory in the early 20th century, the behavior of light was no longer a mystery. The goal became to look for ways to control and manipulate light. Light reflected by mirrors to convey information across large distances was used by the Greeks. During World War II, warships communicated using various codes by modulating spotlights. Simple lab experiments will show that laser light will propagate through a column of water. How does this occur, and can we take advantage of this property to propagate light in any direction we choose, over long distances, without suffering high losses? The answer is yes.

A well known optical illusion is to "bend" a pencil by dipping a pencil in a glass of water. Of course the pencil is not bending, but rather the rays from the pencil are shifted by a small amount due to the difference in the index of refraction. Another example is the view of a swimmer below the surface of the water. As he looks up he will notice a circular area where he can see the sky or perhaps his boat. However if he looks farther ahead, he will notice he cannot see through the surface of the water and in fact, he can see reflections of fish swimming ahead of him. In this case, light is being *totally internally reflected* and it is this effect we wish to exploit to guide light along the path of our choice.

Total internal reflection is a consequence of the boundary conditions imposed by classical electromagnetic theory on the perpendicular and transverse components of an electromagnetic wave . Light entering a low index material from a high index

material will be reflected provided the angle is greater than the critical angle. To illustrate this concept see Figure 2.1(a). The critical angle of the glass-air interface can be calculated by

$$\theta_c = Sin^{-1} \frac{n_t}{n_i} \tag{2.1}$$

where θ_c is the critical angle, n_t is the index of the transmission medium and n_i is the index of transmission of the incident medium. Now imagine we use two glasses with close indices of refraction rather than air and water. We form a cylindrical *core* of glass with a high index of refraction, say 1.53, and a cylindrical *cladding* of glass with an index of refraction of 1.51. Using equation 2.1, we arrive at a critical angle of 1.40 radians. Figure 2.1(b) demonstrates the concept of an optical fiber. A cylindrical glass tube is extruded in long thin strands and doped with various impurities such as Germanium or Phosphorous to create small differences in the index of refraction between the core and the cladding.

Now that we have seen an optical fiber is nothing more than two glasses of differing index of refraction, we can ask the question of *how* we might vary the index of refraction and core size to take advantage of mode structure within the fiber. The index profile can be modeled by Equation 2.2, where r is the distance from the optical axis of the fiber, a is the core radius, n_1 is index of the core, n_2 is the index of the cladding , and p is the *grade profile parameter*.

$$n^2(r) = n_1^2 \left[1 - 2 \left(\frac{r}{a} \right)^p \frac{n_1^2 - n_2^2}{2n_1^2} \right] \tag{2.2}$$

Two methods in common use are the step index and graded index. In a step index fiber the index of refraction profile is step-like and discontinous across the two glasses (p = ∞). In a graded index, the index of refraction profile is a polynomial of degree p = 1 to ∞, but is commonly parabolic (p=2). Each index profile has
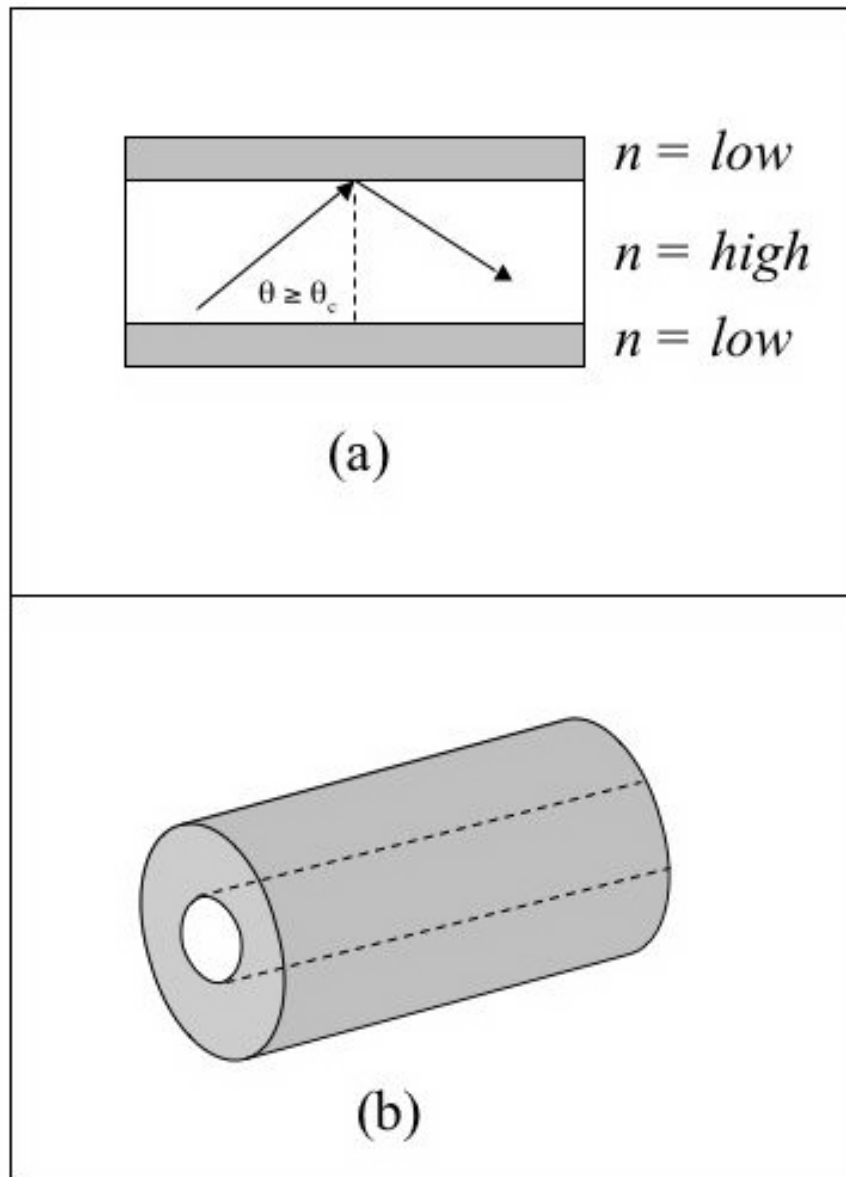
Figure 2.1:   Total internal reflection in a two-dimensional slab
waveguide (a), and the concept of an optical fiber (b).
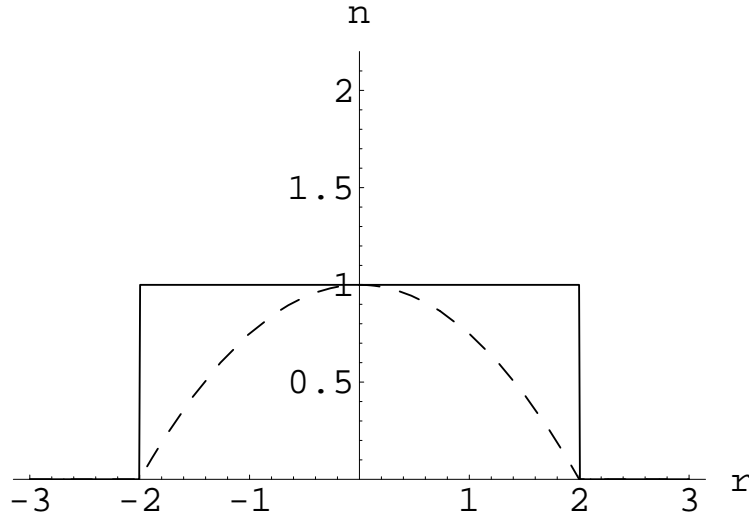
Figure 2.2:   Index profiles for the core of an optical fiber. The solid line is a step index fiber and the dashed is a parabolic graded index fiber with p = 2. Dimensions are relative to the cladding index which is zero.

advantages and both are used in this thesis work. Figure 2.2 shows the index profile for a step index and parabolic graded index fiber.

An important parameter derived from the difference in the indices of refraction is the numerical aperture (NA). The NA can be calculated by

$$NA = \sqrt{n_1^2 - n_2^2} \tag{2.3}$$

where n_1 is the core index of refraction and n_2 is the cladding index of refraction. Alternatively, the NA can be described as the sine of the maximum entry half angle from the optic axis of the fiber.

Core diameter is perhaps the single most important parameter of an optical fiber. Depending on the diameter of the core, the fiber will be either *single-mode* or *multimode* for a give wavelength. Along with the numerical aperture defined above, core diameter allows us to calculate the so-called *V-parameter* which governs the number of modes supported in a fiber. For example, if V is calculated to be less than

2.405, only the fundamental mode of the fiber is permitted to propagate. V may be calculated for step and gradient index fibers by the equation

$$V = 4\pi \frac{d}{\lambda_0} NA \tag{2.4}$$

where d is the diameter of the fiber core (commonly given in microns), λ_0 is the wavelength of light, and NA is the numerical aperture calculated in Equation 2.2. The number of modes in a fiber may be approximated by

$$M \approx \frac{4}{\pi^2} V^2 \tag{2.5}$$

if the fiber is step index or

$$M \approx \frac{V^2}{4} \tag{2.6}$$

if the fiber is a has a parabolic index profile. In both cases V is taken to be much greater than unity.

Depending on the size and shape of an optical fiber, one mode or a superposition of many modes can exist in an optical fiber. Due to the cylindrical symmetry of the fiber, Maxwell's equations may be accurately solved assuming the difference between the index of refraction in the core and the cladding is small, typically less than 0.01. This is called the weakly guided case. [12]. The solutions to Maxwell's equations in this case are the Bessel and modified Bessel functions. These functions provide the mathematical model for the optical modes and are given two indices, the azimuthal mode number, n, and the radial mode number l. Higher order modes give rise to "noisy" beam shapes and poor intensity profiles. Figure 2.3 shows the characteristics of several lower order modes that can be found in an optical fiber. In reality, the fiber used for this research are multimode and support tens of thousands of modes. For the purposes of directing optical energy on a target, the beam shape should be
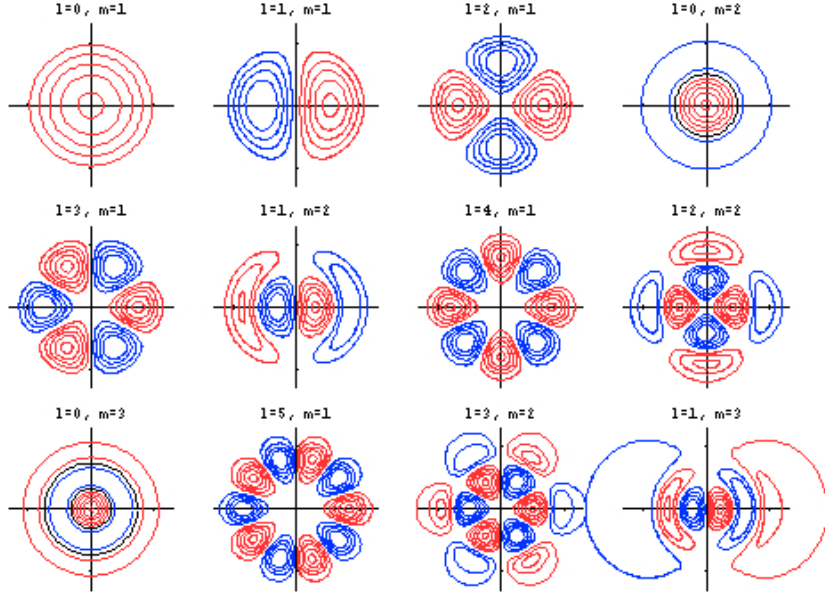
Figure 2.3: Modes of a fiber with a top-hat refractive index profile. The lowest-order mode (l = 1, m = 0, called LP01 mode) has an intensity profile which is similar to that of a Gaussian beam. Note that for a given wavelength, the number of fiber modes is finite; e.g., the figure shows all modes for the given configuration. In general, light launched into a multimode fiber will excite a superposition of different modes, which can have a rather complicated shape. [1]

single-lobed and the beam should diverge as slowly as possible en route to the target to ensure maximum optical fluence downrange. The optimum mode for this situation is the *fundamental* mode, called LP_{01} or HE_{11}. In this mode, the electric field is linearly polarized and orthogonal to the magnetic field. The intensity profile takes on a Gaussian shape as in Figure 2.4. How might we measure beam quality and compare a beam with this ideal shape?

While many methods have been used in the past, perhaps the most widely-known method of measuring beam quality today called M^2 or *mode quality*. M^2 is the factor by which the product of the actual angular divergence and waist size exceed ideal [20]. To calculate M^2, divide the product of the angular divergence of the beam and the waist size (also known as the *beam parameter product*, (BPP)) by the waist size of the diffraction limited Gaussian beam of the same wavelength including divergence. [2]
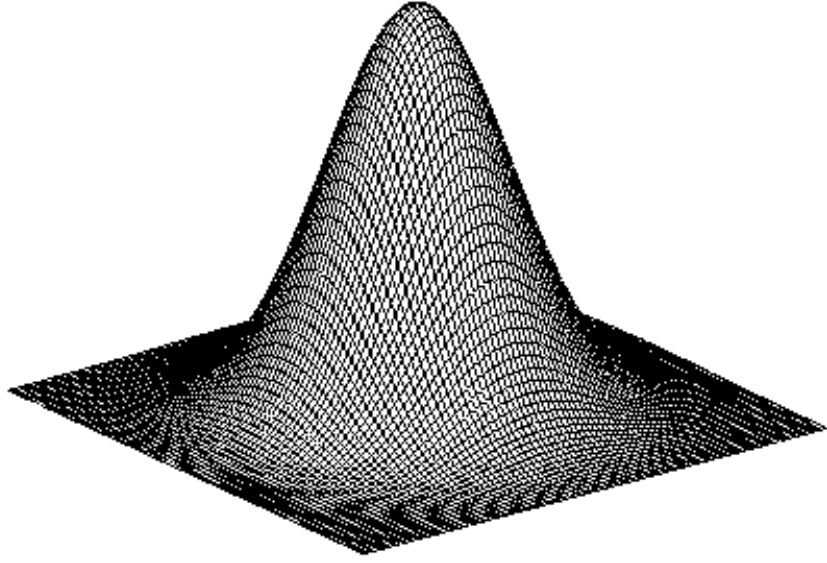
Figure 2.4:   3D plot of a purely Gaussian beam which closely approximates the LP_{01} mode in an optical fiber. [3]

The ideal laser beam has an M^2 of 1. The value of M^2 can be greater than one but is never less than one.

For a Gaussian beam, the beam radius w(z) can be calculated by

$$w(z) = w_0 \sqrt{1 + \frac{z}{z_R}} \tag{2.7}$$

where w_0 is the beam waist, z is the distance from the waist, and z_R is the Rayleigh range. The Rayleigh range is the distance over which the beam may be considered undiverged, but by definition is when the beam radius has increased to $w(z) = \sqrt{2}w_0$. The angular divergence of a Gaussian beam in the far field can by calculated by

$$\theta = \frac{\lambda}{\pi w_0} \tag{2.8}$$

where λ is the wavelength and w_0 is the beam waist

Unfortunately, light does not propagate without losses in optical fibers. Through-put depends on the frequency of the incident light, the dopants used, and the length

10

of the fiber. Typically, the losses are empirically measured by the manufacturer in dB/km at several popular wavelengths. At wavelengths other than those provided, the loss parameter α can be empirically derived or interpolated from a chart. The loss parameter in units of length^{-1} may be calculated empirically by

$$\alpha = \frac{-1}{\ell} \ln \left(\frac{I_t}{I_{lens}\eta_c} \right) \tag{2.9}$$

where ℓ is the length of the fiber, I_t is the transmitted intensity, I_{lens} is the intensity at the coupling lens and η_c is the coupling efficiency of the lens. Once the loss parameter is known, you may calculate the throughput efficiency, η_{fib} of an optical fiber by the formula

$$\eta_{fib} = \frac{P_{out}}{P_{in}} = \exp \left[\frac{-\alpha^*}{4.343} \ell \right] \tag{2.10}$$

where P_{in} is the power measured going into the fiber, ℓ is the length of fiber in kilometers, and α^* is the loss in dB/km. Another useful figure of merit for optical fibers is effective length. This is the interaction length an optical photon sees due to losses. Two fibers of different length may have the same effective length. It may be calculated by

$$L_{eff} = \frac{1}{\alpha} \left(1 - \exp \left[-\alpha L \right] \right) \tag{2.11}$$

Successfully manipulating the path of light requires knowledge of its polarization and the effects of individual components on the polarization. In many experiments the design is based on the ideal situation where polarization is always fixed. This is seldom realized on the lab table! In theory, light propagated through a circular fiber maintains its polarization. If it enters the fiber with vertical polarization it should remain that way upon exiting. However, due to many factors, including temperature variations within the fiber, strain induced birefringence, and random noise from the input source, elliptical polarization is usually observed at the output. Despite the

fact that the overall power measured at the fiber output is not affected, the ability to control the output with beamsplitters and polarizers is hampered by the presence of elliptical polarization.

To combat the formation of elliptical polarization, special *polarization maintaining* (PM) fiber is used. PM fiber can be constructed several ways, but it general, it relies on creating different propagation constants for the orthogonal polarization components. This can be done by using an elliptical core or inducing asymmetric strain in the core . This experiment utilized a PM fiber that employed the latter method by placing two glass rods with different thermal expansion coefficients in the cladding. Figure 2.5 provides an illustration of this method. During the cooling process the rods stress the glass in a way that creates a birefringence condition in the core. This birefringence allows the electric field vector that is parallel to the stress rods to propagate and the other to be attenuated. For the reader unfamiliar with the concept of birefringence, a good introduction may be found in chapter 8.4 of [10, pp. 336-344].

2.2   *Stimulated Brillouin Scattering*

If the electric field inside a fiber becomes intense enough, nonlinear effects will arise due to changes in the material's dielectric properties. Stimulated Brillouin scattering is a nonlinear effect created by the scattering of a photon off an index variation created by an acoustic field. If the acoustic wave is generated by the application of an external field, then the scattering process is considered to be *simulated*. A schematic representation of the energy relationship for SBS may be found in Figure 2.6. A photon annihilates and creates an acoustic phonon and a redshifted photon traveling in the *opposite* direction.

This process must conserve energy and momentum of the respective photons and phonons. The three waves are therefore related by
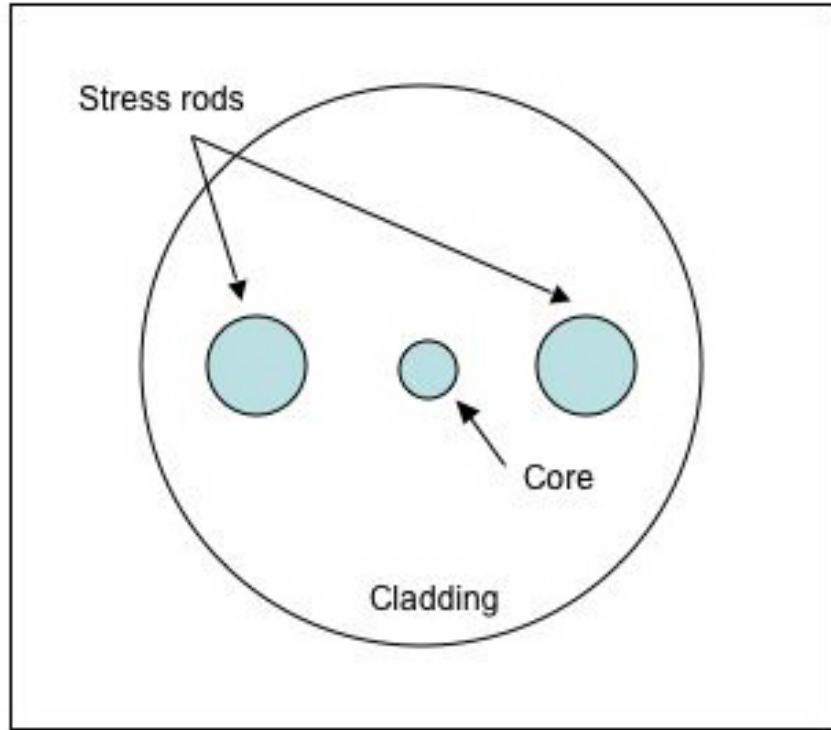
Figure 2.5:   Stress rods in a PM fiber. The stress rods create an induced birefringence that allows only one polarization to propagate.
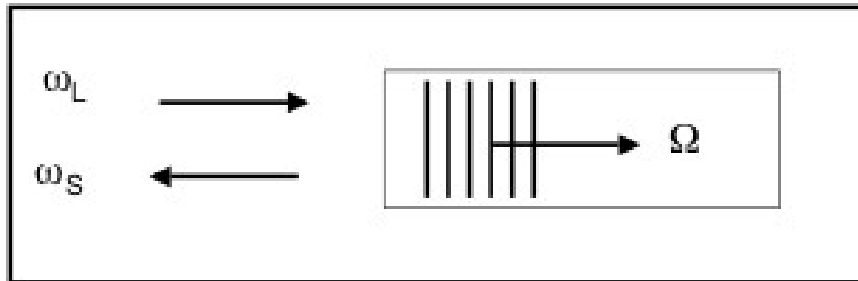

Figure 2.6:   Energy diagram of SBS in an optical fiber. An acoustic phonon Ω is created by the annihilation of a photon ω_L and creates a redshifted optical photon ω_S traveling in the opposite direction.

$$\Omega = \omega_L - \omega_S \tag{2.12a}$$

$$\mathbf{k}_\Omega = \mathbf{k}_L - \mathbf{k}_S \tag{2.12b}$$

where $\mathbf{k}_\Omega$ is the propagation vector of the acoustic phonon, $\mathbf{k}_L$ is the propagation vector of the source photon that is annihilated, and $\mathbf{k}_S$ is the propagation vector of the redshifted Stokes photon.

Electrostriction is the tendency of a material to compress in the presence of an electric field. A change in the density of the material causes changes to the optical properties of the material. The change in the susceptibility of the material can be calculated by

$$\Delta\chi = \frac{1}{32\pi^2} C \gamma_e^2 \langle \tilde{\mathbf{E}} \bullet \tilde{\mathbf{E}} \rangle \tag{2.13}$$

where $\Delta\chi$ is the change in susceptibility, C is the material compressibility, γ_e is the electrostrictive constant, and $\tilde{E}$ is the applied electric field. This change in susceptibility leads to a change in the polarization vector in the material

The pump beam and spontaneously scattering light cause the fiber responds harmonically, creating an acoustic wave which accounts for the interaction between the pump and Stokes beam which was created from thermal noise.

$$\tilde{\rho}(z,t) = \rho_0 + [\rho(z,t)\exp[\imath(qz - \Omega t)] + c.c.] \tag{2.14}$$

where ρ_0 is the unperturbed density, q is the acoustic wave vector, Ω is the frequency of the acoustic wave, and c.c. is the complex conjugate. [6, p. 418] This pressure wave acts as an acoustic Bragg grating throughout the length of the fiber. This grating scatters light according to Bragg theory and generates a Stokes beam traveling in the

opposite direction that is redshifted on the order of tens of GHz. The Brillouin shift may be calculated by

$$\nu_B = \frac{2n\nu_A}{\lambda_p} \tag{2.15}$$

where ν_B is the Brillouin shift, n is the index of refraction, ν_A is the acoustic velocity, and λ_p is the wavelength of the pump source. [4, p. 265]

Once the system has reached steady state and we make the slowly-varying amplitude approximation, the amplitude of the Stokes and pump waves may be modeled by two coupled-amplitude equations

$$\frac{dA_1}{dz} = \frac{\imath q^2 \gamma_e^2}{8\pi nc\rho_0} \frac{|A_2|^2 A_1}{\Omega_B^2 - \Omega^2 - \imath\Gamma_B} \tag{2.16a}$$

$$\frac{dA_2}{dz} = \frac{-\imath q^2 \gamma_e^2}{8\pi nc\rho_0} \frac{|A_1|^2 A_2}{\Omega_B^2 - \Omega^2 + \imath\Gamma_B} \tag{2.16b}$$

where A_1 is the amplitude of the pump, A_2 is the amplitude of the Stokes, ω is the frequency of the Stokes and the pump, γ_e is the electrostrictive constant, n is the index of the material, c is the group velocity, Ω_B is the Brillouin frequency, Ω is the acoustic wave frequency, and Γ_B is the Brillouin linewidth. [6, p. 420]

Assuming exponential decay of the acoustic waves in the fiber, SBS has a Lorentzian gain profile and the gain may be calculated by

$$g = g_0 \frac{(\Gamma_B/2)^2}{(\Omega_B - \Omega)^2 + (\Gamma_B/2)^2} \tag{2.17}$$

where g_0 is the line-center gain factor

$$g_0 = \frac{\gamma_e^2 \omega^2}{nvc^3 \rho_0 \Gamma_B} \tag{2.18}$$

The line-center gain factor may be used to estimate the power required to reach SBS threshold by the equation

$$P_{thresh} \approx 21 \frac{A_{eff}}{L_{eff} g_0} \tag{2.19}$$

where A_{eff} is the effective area of the fiber. The effective area can be approximated by the true area of the fiber core or empirically measured [11]. Typical effective areas in optical fibers range from 20-125,000 μm^2

Conversely, the Brillouin gain g may be estimated by rearranging the above equation and solving for g. The factor of 21 can be doubled depending if the polarization of the pump and Stokes are mixed [4, p. 269]

The solutions of equation 2.16 lead to an intensity relationship between the pump and Stokes fields [4, p. 268] that are valid after the Stokes wave is created

$$\frac{dI_s}{dz} = -gI_p I_s + \alpha I_s \tag{2.20a}$$

$$\frac{dI_p}{dz} = -gI_p I_s - \alpha I_p \tag{2.20b}$$

where the α term includes the losses in the fiber for both the pump and Stokes.

Equations 2.20 can be solved one of two ways. For estimating the intensity of the Stokes wave near threshold, one can neglect pump depletion. The solution therefore is

$$I_s(0) = I_s(L) exp \left(\frac{g P_0 L_{eff}}{A_{eff} - \alpha L} \right) \tag{2.21}$$

which describes an exponentially growing Stokes wave traveling in the backward direction. If the pump depletion is taken into account, then another method must be used. [4, p. 269]

2.3 Historical Considerations

In this section the reader will be given a short history of the experiments and results that precede this thesis and the important results derived from them. Only works dealing with stimulated Brillouin scattering in optical fibers are considered. For a larger perspective of SBS, including Brillouin lasers, amplifiers, and phase conjugation, see [4, 21].

SBS was first demonstrated in optical fibers by Ippen and Stolen in 1972 [11]. In this seminal work, Ippen and Stolen utilized a pulsed Xenon laser at 535.5 nm that contained an internal etalon to reduce the linewidth to less than 100 Mhz. Two important results came from this work. First, a narrow linewidth is essential for reducing the SBS threshold to less than one Watt. Second, the use of single-mode fibers to stimulate the fundamental mode and encourage rapid growth of the Stokes beam. Ippen and Stolen concluded that SBS was more of a problem than originally thought by telecommunications experts because the Stokes wave could grow to such intensity that fiber damage could result. Y. Aoki and K. Tajima showed that in long single-mode fibers, the threshold could be as low as 13 mW in a 10 km optical fiber [5]. Until the late 1980's, most work on SBS in optical fiber concentrated on reducing the effect in order to limit the damage to, and interference in, telecommunications circuits.

During the later years of the Cold War, researchers in the United States and the former Soviet Union attempted to exploit SBS for various defense applications such as phase conjugate mirrors, beam combination, and beam cleanup. Sternklar, *et. al.* demonstrated that to combine two beams into an optical fiber with a spherical lens using stimulated Brillouin scattering, the alignment bandwidth is on the order of 1 mrad. [19]. Further, the two beams can excite their own Stokes beam which only overlap in the Gaussian tail. Sjöberg showed that the CW SBS threshold in short multimode fibers increased with decreasing input beam quality. He also showed that the generation of SBS is affected by mode mixing as the beam quality degrades down the length of the fiber [18]. Beam cleanup in long, multimode fibers was shown to be

feasible by Brusselbach which was a major source of inspiration for this thesis. Figure 2.7 shows the clean-up power vs input power [7]. Furthering this concept, recent work at AFIT [14, 16, 17] demonstrated beam combination and cleanup of two coherent beams in long multimode fibers as well as two incoherent beams.
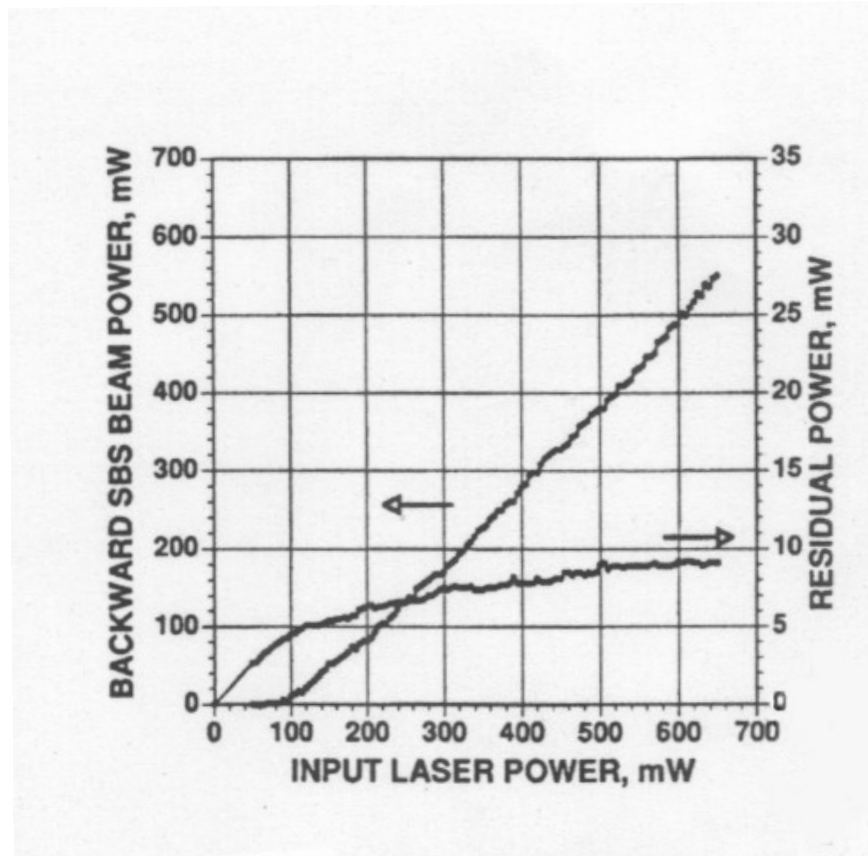
Figure 2.7: Cleaned-up power vs Input Power in a multimode optical fiber. The fiber used was a 3.3 km V=14.4 step-index silica fiber. [7]

III. Experimental Methods and Equipment

C HAPTER III outlines the methods and equipment used to investigate beam com-
bination in long multimode optical fibers. First, the methodology for amplifi-
cation of a narrow linewidth signal will be presented. Second, the characteristics of
SBS in optical fibers will be described. Lastly, a description of the equipment and
procedures required to evaluate off-axis beam combination is provided.

3.1   Fiber Amplifier and Channel Division

In order to generate SBS, a narrow linewidth source is required as discussed
in Chapter II. High power is a secondary requirement if generating SBS via off-axis
marginal rays, and many commercial sources with narrow linewidth at 1.06 μm do
not provide sufficient power. In order to satisfy both requirements, a Ytterbium-
doped fiber amplifier was used to boost the output of the seed laser to 10 Watts. The
seed laser used was a Lightwave Electronics, Inc. Series 125 Nd:YAG Non-Planar Ring
Oscillator (NPRO) which outputs a 700 mW signal at 1.06 μm with a linewidth of less
than 5 kHz. The NPRO output was collimated and focused into a Nufern 10.33 meter
polarization maintaining, Ytterbium-doped fiber using a 10x microscope objective. A
Lissotschenko Mikrooptik (LIMO) LDD-50 semiconductor diode laser array at λ=975
nm was backwards fed into the fiber amplifier by a 20x microscope objective. The
details of the fiber amplifier can be found in Figure 3.1.

The output polarization of the amplifier was fixed by aligning the stress rods
in the fiber with the polarization of the NPRO seed beam. The stress rods impart
a natural birefringence in the fiber that allows the fiber to maintain polarization.
This is important because the beamsplitters used to equally divide power required the
input to be p-polarized. Secondly, it allows control of the pump and Stokes beams
using polarization beam splitters. The polarization of the seed beam was controlled
by a half-wave plate on the exit aperture of the Faraday rotator. To ensure the correct
polarization a beam splitter cube was used to determine the polarization at the output
of the fiber amplifier. By iterating both the angle of the input and output half-wave
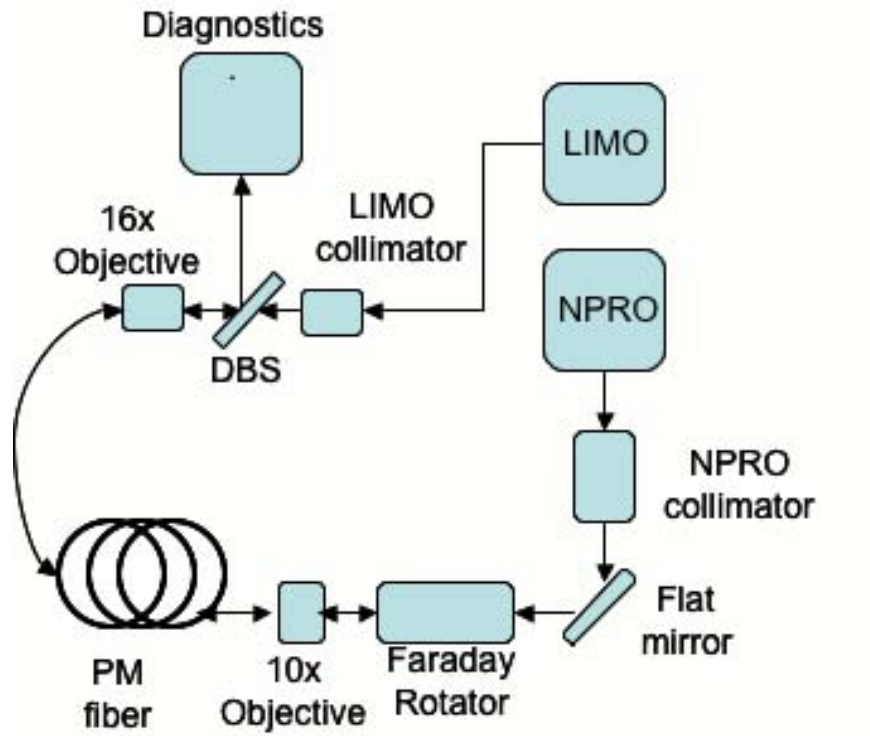
Figure 3.1:   Fiber amplifier layout. A dichroic beamsplitter (DBS) was used to separate the pump from the signal. The Faraday rotator contains two half-wave plates for adjusting the polarization of the NPRO seed.

plates, p-polarized output was achieved. The output of the fiber amplifier was spatially filtered using a 1mm pinhole to reduce the amount of elliptically polarized light from the cladding of the PM fiber from entering the beam combiner. The wavelength spectrum of the fiber amplifier is shown is figure 3.2. The actual linewidth is much smaller due to optical spectrum analyzer resolution, and estimated to be less than 80 Mhz. The maximum observed power of this fiber amplifier was 9.3 Watts at an input power of 25 Watts. The M^2 value of the amplified signal, taken at an output of 651 mW, was ≤ 1.5. The M^2 value at higher powers was predicted to remain good due to the single-mode core of the fiber amplifier. The M^2 value was calculated with a ModeMaster beam propagation analyzer.

Two methods of channel division were used. The first method was used to demonstrate generation of the Stokes beam using four off-axis side channels with no center seed. The second method used a center seed beam and the off axis rays to investigate the interplay of the seed and side channels. Figure 3.4 details the experimental setup with no seed beam. The 1.06 μm output of the fiber amplifier was split by a dichroic beam splitter and then distributed into four channels using standard flat mirrors coated for the near infrared band. The channels were focused into 9 μm single mode pigtail collimators using Optics For Research (OFR) fiber ports. The pigtail collimators have gradient index (GRIN) lenses (focal length = 5.00 mm) cemented to the ends to provide collimated output. Figure 3.5 shows the "Gatling gun" fiber mount (GGM). The GGM was an aluminum disk with six holes drilled around a central hole of diameter 3 mm, which is three times larger than the calculated fundamental mode beam waist of the Stokes return beam from the 62.5μm fiber.

The beam combiner concept is shown in figure 3.6. This configuration of the holes was designed to provide a minimum entry angle into the fiber but still allow the possibility of a Stokes beam to return through the center. The collimated output is directed to a 15 mm focal length gradient lens that focuses the four channels into the core of a long multimode fiber which is clamped into a rotary fiber chuck and

x-y translation stage. Both the lens and beam combiner have tip-tilt adjustment in addition to x-y translation.

A center seeded configuration was used to evaluate the effects of the side channels on the center seeded Stokes beam. Figure 3.7 details the experimental setup. The output of the amplifier is passed through a spatial filter and then two beamsplitters. These beamsplitters create two branches of relatively equal power and a center channel that is used to seed the Stokes beam. In this setup, the center channel is passed through another half-wave plate and then a polarization beamsplitter cube (PBS) that directs the seed into the SBS fiber. The side channels are passed through the polarization beam splitter cube and then focused using the gradient lens into the SBS fiber. To monitor the SBS created by the center seed channel, a glass microscope slide was used to pick off a small portion of the return beam. The polarization of the side channels was oriented 90 degrees with respect to the center channel. Any Stokes generated by the side channels should return through the polarization beam splitting cube and the center of the beam combiner. The objective was to show that the side channel and the center channel formed two Stokes beams. Both Stokes beams were analyzed with a Burleigh scanning Fabry- Perot etalon and a Newport diode detector power meter.

3.2   Characteristics of SBS in Optical Fibers

Two different fibers were evaluated for production of SBS. Both fibers were multimode. The first fiber was a gradient index OFS, Inc. silica fiber with a core diameter of 62.5 μm and a cladding diameter of 125 μm. The second fiber was a gradient index OFS, Inc. silica fiber with a core diameter of 100 μm and a cladding diameter of 225 μm. Each fiber was tested for its ability to couple up to four channels from the beam combiner. To perform this test, a length of fiber approximately one meter was cut and the ends cleaved at zero degrees using a 3SAE Auto Prep II fiber cleaver. Output power was measured at the end of the fiber compared to and plotted against the input power. This test is important because the ability to efficiently

couple multiple beams will vary depending on the number of beams being combined and size of the fiber. The tradeoff is made between having a small fiber with a low SBS threshold and a larger fiber that will accept more light.

Once the coupling efficiencies were measured, the full length of fiber was evaluated for creation of a Stokes beam. The two fibers tested had different lengths and loss characteristics. The 62.5 μm fiber was 8.8 km long and had an estimated loss of 1.2 dB/km. The 100 μm fiber was 4.4 km long and had an estimated loss of 2.0 dB/km based on a chart provided by the manufacturer. To provide a sense of the coupling efficiency while using the long fibers, the path losses were calculated and compared to experimental data. It was important to ensure all channels were contributing equally and coupling into the fiber. While maximizing the observed output is helpful, it is much better to cover one channel at a time and determine what percent of each channel is actually being coupled into the fiber. This method ensured that one channel was not solely generating SBS.

In order to provide a gauge of the power level required to generate SBS, each fiber was tested by launching a beam down the optical axis which allowed the best chance for the generation of the fundamental mode. This was done using the center seeded configuration in Figure 3.7 with power measurements taken in front of the gradient lens and at the end of the fiber under test. Recall from Chapter II, the center-seeded geometry has the theoretical lowest threshold for SBS generation and will be a bellwether for evaluating the SBS threshold required for the off-axis beams. The input power, output power, and reflected (Stokes) power were measured and the SBS conversion efficiency was calculated.

3.3 Off-Axis Beam Combination

Perhaps the most important aspect of this thesis was to demonstrate the ability to generate SBS using only multiple side channels which are offset from the optical axis of the fiber. Using the first configuration (Figure 3.4), the side channels were aligned with the front face of a 15 mm gradient lens that focused the four beams into the

fiber. In preparation for investigating SBS with a center seed, a second configuration was also used in a separate experiment as shown in Figure 3.7 but by blocking the center channel. The results of the two configurations will be discussed in Chapter IV.

Due to the use of only four of the possible six beams in the GGM, the beam spots took the form of a diamond shape. The orientation of the beam asterism created by the GGM was not uniform due to the fact that the GGM was hand assembled and the pigtail collimators held in place with five-minute epoxy. Even though the gradient lens is designed to limit the effects of spherical aberration created by the imperfect positioning of the side channels, it was important to orient the beam asterism in a way that maximized coupling into the SBS fiber. This was done using a process of trial and error by rotating the beam combiner in its mount and then using the translation stages of the SBS fiber to minimize the scattered light due to poor coupling from the fiber's front facet, while simultaneously maximizing the residual power measured at the back end of the SBS fiber.

Once the fiber and side channels were properly aligned, a power meter was placed in front of the beam combiner and power reading were taken using a 30 Watt Newport detector head power meter. These results were mapped to the drive current of the LIMO diode pump laser and used for later calculations. A Burleigh scanning Fabry Perot spectrometer was placed directly behind the center opening of the beam combiner to view the reflected beam and indicate the presence of SBS. Beginning at the lowest drive current that produced a quality beam, the drive current was increased one amp at a time and the output of the etalon was viewed on a LeCroy LC584AM oscilloscope. If a Stokes beam was observed a power meter was inserted to measure the reflected power. Due to the fluctuations observed in the Stokes beam, a LaserProbe RM-6600 Universal Radiometer was used to take energy readings in addition to the average power readings taken earlier.

After the Stokes measurements were taken, the contribution of each side channel was assessed. At a high and low input power, the residual throughput of the SBS fiber

was measured. Each channel was blocked using an opaque object and the residual throughput power was measured. The actual and percent contribution of each channel was calculated and if the sum of the contributions was not within the one sigma error of the initial residual throughput, another measurement set was taken. After taking these measurements with the full length of SBS fiber, approximately one meter of the SBS fiber was cut and the test repeated. For the one meter test, the effective coupling efficiency of the beam combiner was also calculated.

3.4 Off-Axis Beam Effects on the Center Channel

While the importance of generating a Stokes beam using the only off-axis side channels was the main focus of this research, the interplay of the side channels and a center seed beam was also characterized. Previous work [9] showed that it was possible to couple up to 16% of the side channels to a Stokes beam created by the center channel. Because of the complicated mode structure created by the side channel due to the geometry of entry into the SBS fiber, the effect on the Stokes beam created by the center seed beam was investigated.

Using the configuration in Figure 3.7, a center seed beam was directed to the front surface of the gradient index lens using a polarization beam splitting cube. The input beam asterism from the beam combiner was also passed through this cube along with a half-wave plate. One difficulty with this setup is that the alignment of the center beam fixes the position of SBS fiber. This leaves only the x-y tilt adjustments and the rotation of the beam combiner to satisfactorily combine the side channels. In this configuration the effect of *one* side channel was demonstrated due to the difficulty of aligning four beams through the PBS cube. Once the side channel and center seed beam were aligned an average power reading was taken in front of the gradient index lens as the drive current was adjusted. The etalon was positioned after the glass slide pickoff and a power meter was placed behind the center hole of the beam combiner.

3.5 Stokes Beam Quality

An important measure of merit for any laser system is the M^2 value. The importance of this parameter is discussed in Chapter II. To empirically determine the M^2 value of the reflected Stokes beam, I used a near-infrared CCD camera and a 300 mm focal length positive spherical lens on an optical rail. The rail was placed about half a meter from the back of the beam combiner. A half-degree wedge was used to direct the Stokes beam into an alignment pinhole at the front of the rail. The alignment pinhole was replaced with the spherical lens once rough alignment was performed.

After the Stokes beam was centered in the camera's output display, a rough beam waist was found and defined as the center reference point. From the center point, the camera was translated through 5 centimeters on either side of the center. All analysis was performed using Beam Profiler software. Beginning at the -5 cm point on the rail (to the left with respect to the observer), the camera was moved in 0.5 cm increments and the horizontal and vertical beam waist were measured by the software. Because the Stokes beam was intermittent, a ten sample average of the beam waist was performed by the capture software running in pulsed mode. The beam waist averages, along with the camera position were fed into a Mathematica® nonlinear fit routine that calculates the M^2 value and the radius of the beam at the beam waist. Images of both the near field and far field Stokes beam were taken through the camera.

3.6 Chopped Input Beam Combination

To investigate whether or not the intermittent Stokes beam was affected by the input beam shape, a beam chopper of unknown specifications was found and disassembled in the lab. The dimensions of the beam chopper rotor are shown in Figure 3.8. The motor was labeled as 1300 rpm. Using the dimensions of the beam chopper rotor, the angular frequency, f is 21.6 rev/s with a period T of 46.2 ms. Because there are six slots on the chopper blade, the actual period is 7.7 ms which results in a pulse rate of 130 Hz. The angular velocity is calculated by $\omega = 2\pi f$ and

is found to be 136 rad/s. The pulse duration may be calculated by first finding the linear velocity using

$$v = r\omega \tag{3.1}$$

and then using the width of the chopper slot to calculate the duration of the beam during each pass. Using a slot width of 1.9 cm and a linear velocity of 1036 cm/s the pulse duration is calculated to be approximately 1.83 ms.

The beam chopper was inserted at the point just before the pinhole in Figure 3.7. Instead of a power meter, a Joule meter was placed behind the beam combiner to measure the energy of the Stokes beam pulses. These values were then compared to the pulses of the Stokes beam when the beam was not chopped. Additionally, the residual power was measured at the rear of the SBS fiber and compared to the unchopped case.
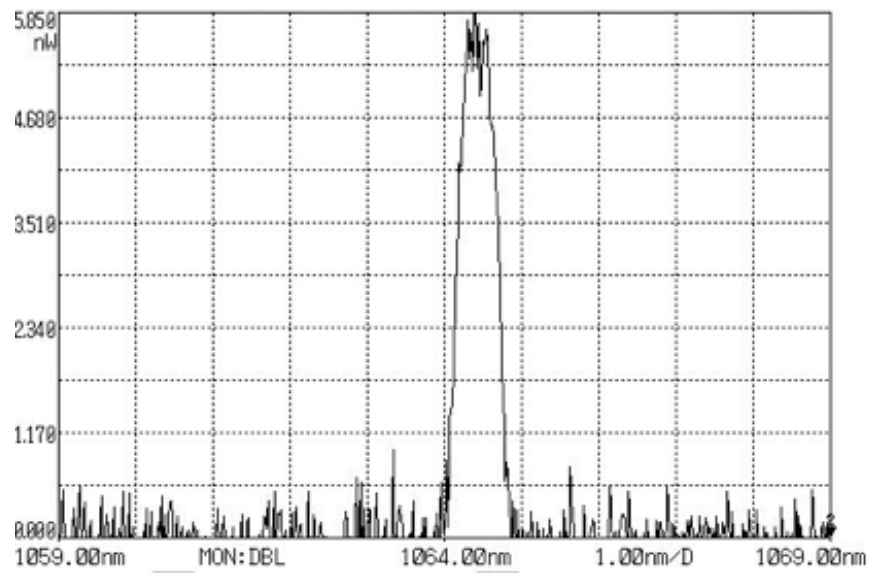
Figure 3.2: Fiber amplifier spectrum. The true linewidth is estimated at 80 Mhz based on measurements taken with the etalon. The best resolution of the spectrum analyzer was 0.5 nm/div.
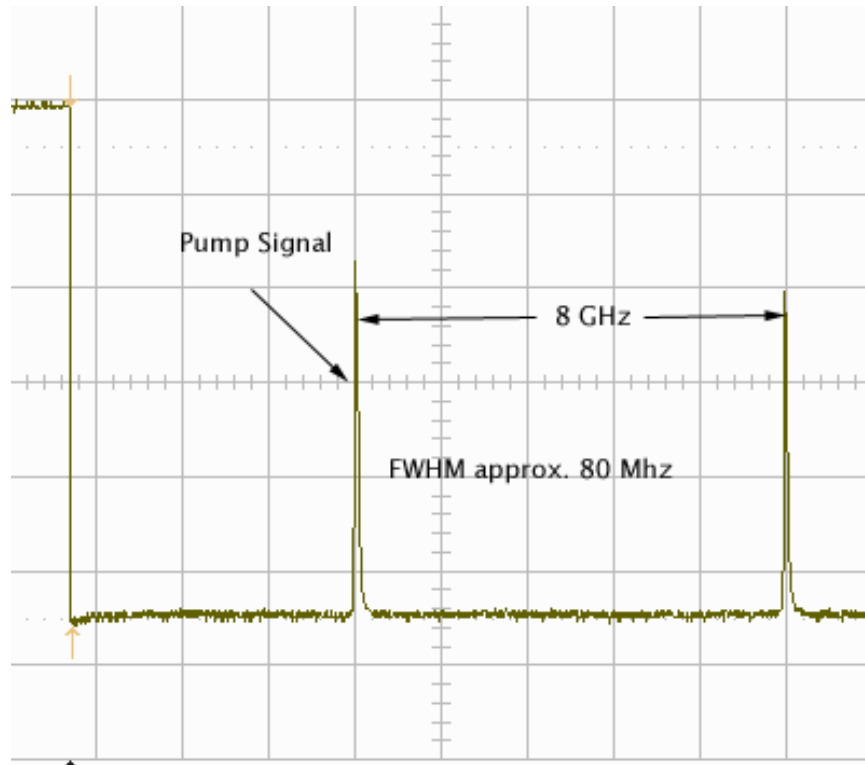
Figure 3.3:   Fiber amplifier linewidth as measured by a Fabry-Perot etalon. The free spectral range of the etalon is 8 GHz and there are 0.32 GHz/division. The linewidth is estimated at less than 80 Mhz.
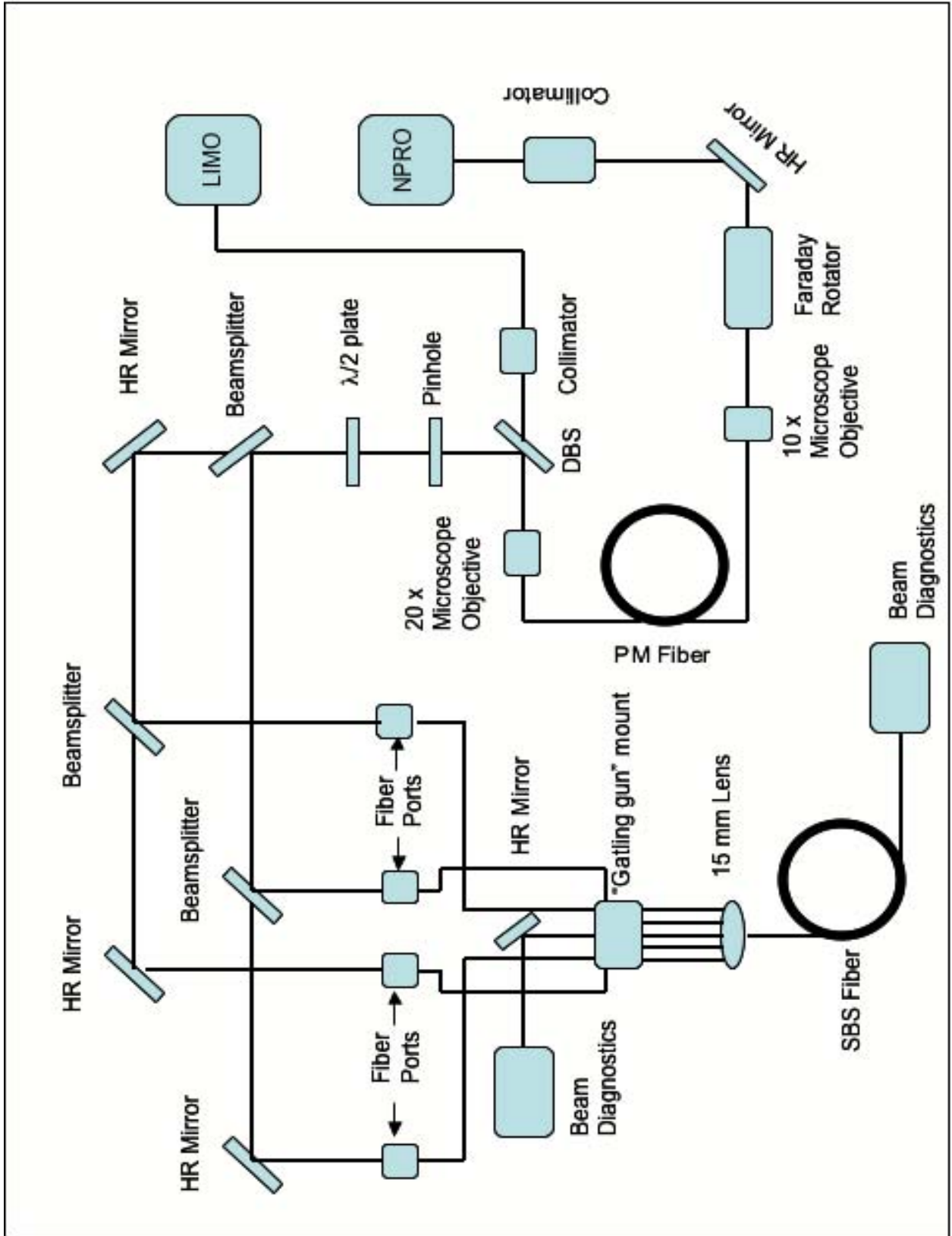
Figure 3.4:   Seedless Experimental Setup. A glass pickoff is
inserted behind the beam combiner to intercept the returned
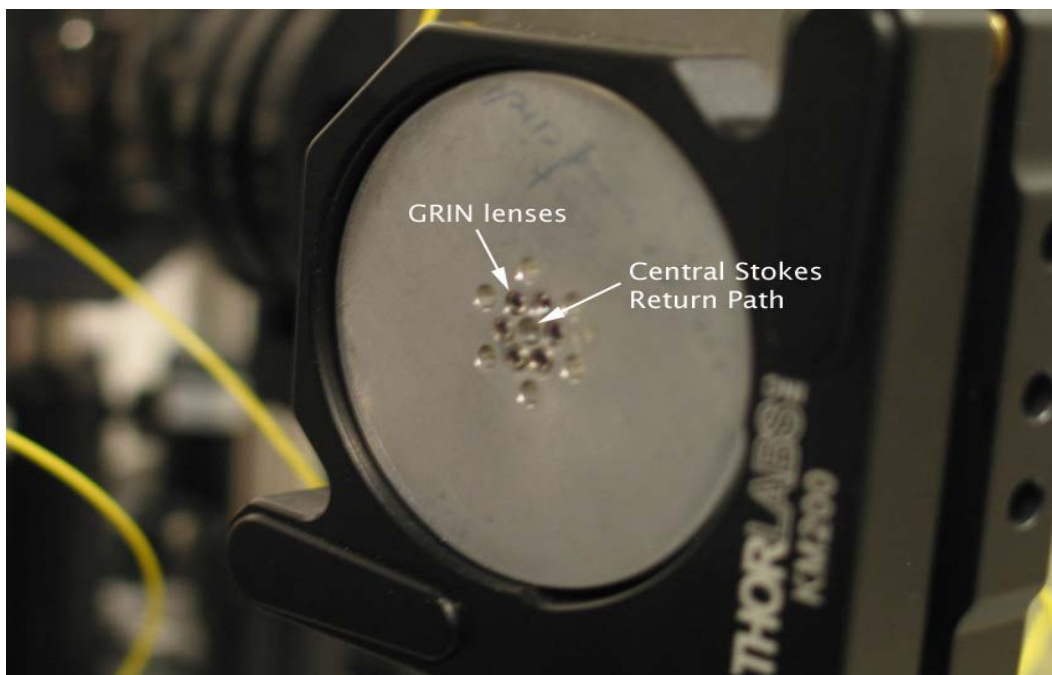Stokes beam.   31

Figure 3.5:   GGM close up photo showing Stokes return path and GRIN lenses surrounding the central hole. Central hole size drilled to fully accommodate returning Stokes beam without vignetting.
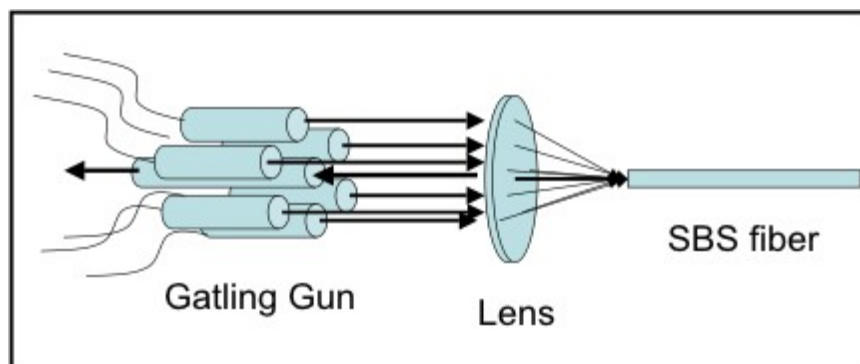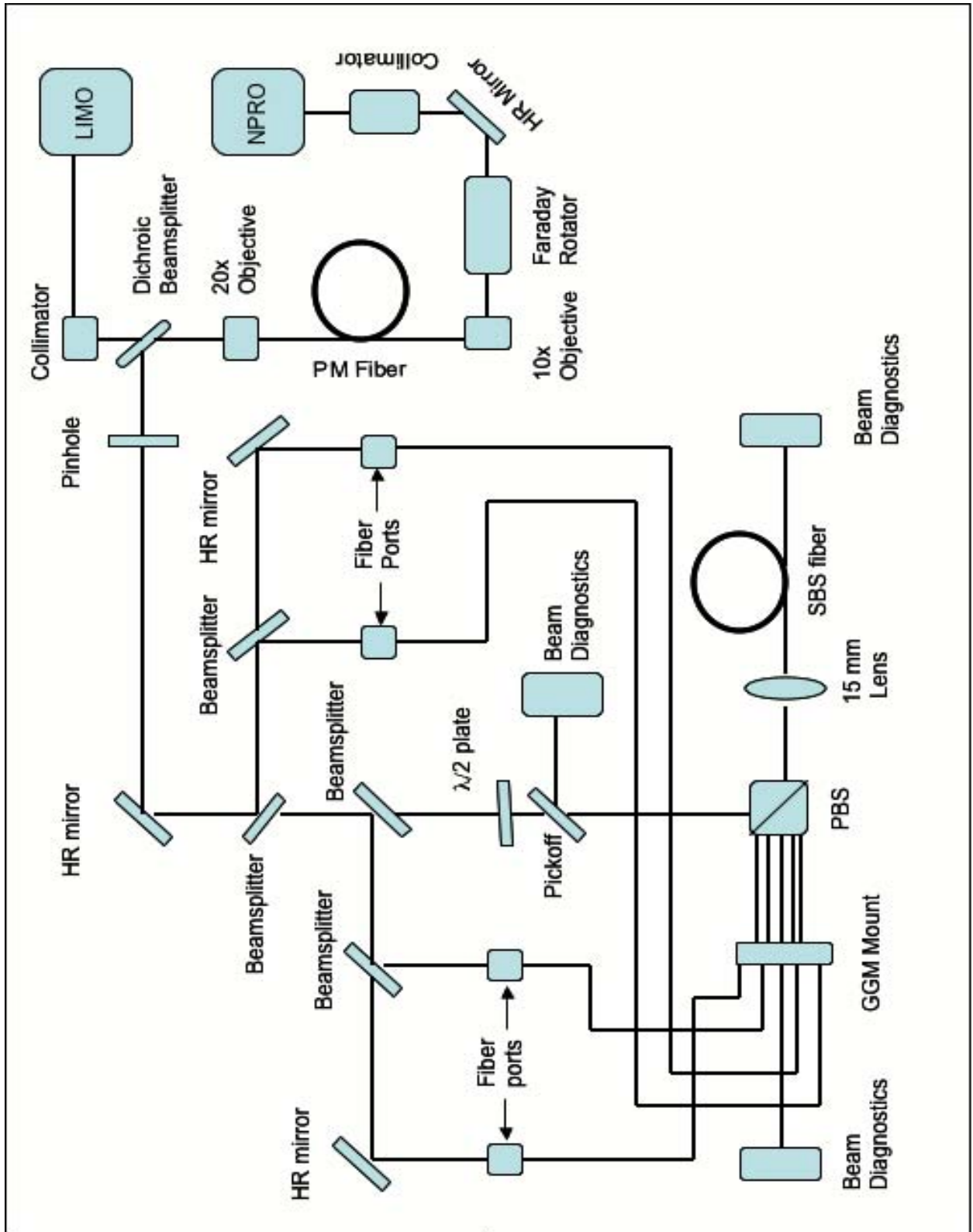

Figure 3.6:   GGM conceptual schematic.

Figure 3.7: Center Seeded Experimental Setup. All optics coated for 1.06 μm. The central channel is blocked during seedless operation.
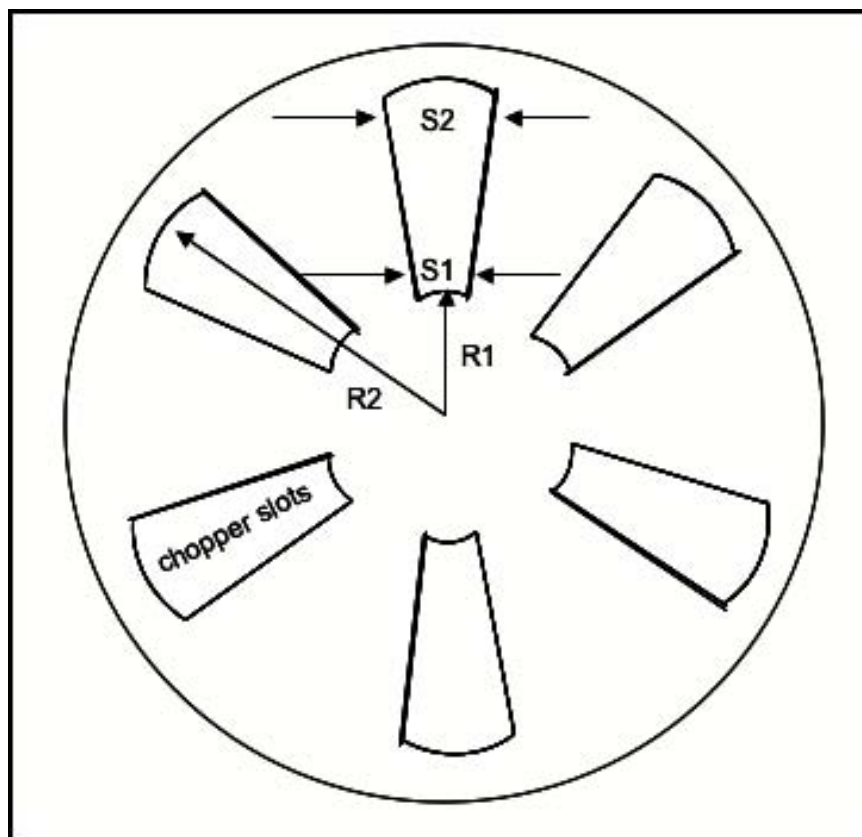
33

Figure 3.8: Beam Chopper Schematic. R1 is 38.1± 0.8 mm, R2 is 88.9±0.8 mm, S1 is 9.52±0.8 mm, and S2 is 22.2±0.8 mm

IV. Results and Analysis

4.1 Characterization of SBS in Multimode Optical Fibers

THE coupling efficiency and SBS threshold of the fibers tested was an important benchmark for this experiment and served as a bellwether for the input power required to test the ability of the beam combiner to produce a Stokes beam. The following is a short summary of the results. The reader unfamiliar to SBS generation is encouraged to read these results for better understanding of the power levels involved.

Recalling from Chapter II, the threshold for SBS when launched down the optical axis can be very low. Depending on the diameter and length of the fiber the threshold value is usually in the tens of milliwatts. When the beam combiner experiment was previously run at AFIT, the SBS threshold for the 62.5 μm fiber was 75 mW, and the 100 μm fiber was 300 mW. [9] What is important to remember is that the SBS threshold will go up as the fiber becomes larger. A larger core also allows you to combine more beams, which presents the researcher with a dilemma. According to Equation 2.19 the predicted P$_{thresh}$ value for the 62.5 μm fiber is 390 mW. Using the center seeded configuration the 62.5 μm fiber was found to have a SBS threshold of 190 mW, which is significantly higher than previously reported. This can be attributed to a difference in the quality of input beam used, and the abberations caused by the PBS cube. For example, using an abberated input, Russell [15] found the SBS threshold in a 4.4 km 50 μm graded index fiber to be 420 mW.

The Stokes conversion efficiency for the 62.5 μm fiber was calculated to be 38%. The power input, measured at the point directly in front of the Gatling gun mount, and power reflected from the SBS fiber, are plotted in Figure 4.1. Compare with Figure 2.7 which is from a 3.3 km V=14.4 step index fiber. The Stokes conversion efficiency for the 62.5 μm graded index fiber is comparable to Russell's $\approx$ 25% but short of the 83% reported by Brusselbach [7]. It is clear that step-index is a better choice for SBS conversion, however numerical aperture must also be considered. The 100 μm fiber did not produce SBS because the center channel was not able to reach

a power above threshold. A decision was made to use only the 62.5 μm fiber due to the high threshold required for the 100 μm fiber.

The Brillouin offset of each fiber was calculated. Assuming an acoustic velocity of 5.96×10^3 m/s, an index of refraction of 1.45, and a pump wavelength of 1.064 μm, equation 2.15 provides an offset of 16.24 GHz for the 62.5 μm and the 100 μm fiber. Each set of Stokes signal is separated by approximately 8 GHz, the free spectral range (FSR) of the etalon. The Brillouin shift is twice the FSR plus the distance from the pump to the Stokes signal. Each horizontal division on the oscilloscope screen represents approximately 3.1 GHz. Therefore, the Brillouin shift was measured to be about 17.5±0.60 GHz. The relative error of the measured Brillouin shift is 7.7%. Using the Brillouin shift, we can arrive at a reasonable approximation of the speed of sound in the fiber. Using Equation 2.15, and assuming an index value of 1.45, the acoustic velocity in the fiber is 6.42×10^3±220 m/s. Assuming a value for the Brillouin gain, g_b, of 5×10^{-11} m/W [4, p. 269], an effective area equal to the core area of 3,066 μm^2, and an effective length of 3.3 km, equation 2.19 predicts the critical pump power P$_{thresh}$, to be 390 mW.

In order to couple in maximum power and ensure that all beams are contributing to the Stokes beam, the efficiency was calculated using the method described in Chapter III. The 62.5 μm fiber was able to couple in 61% of the power from the beam combiner, and the 100 μm fiber was able to couple in 88% of the power from the beam combiner. Using fiber coupling theory, we can calculate the theoretical amount of power that will be combined into the SBS fiber. The 62.5 μm fiber has a numerical aperture of 0.275 and the 100 μm fiber has an numerical aperture of 0.294. Using the geometry of the beam combiner we can calculate its numerical aperture and arrive at a estimated coupling efficiency. The pigtail collimators are 3 mm from the optical axis and assume they are exactly parallel until intersecting the front of the gradient lens. The distance of the gradient lens from the SBS fiber is approximately 15 mm. Including effects from the marginal rays of the individual pigtail beams, the NA of the GGM and gradient lenses is calculated to be 0.233. Theoretically, one can couple
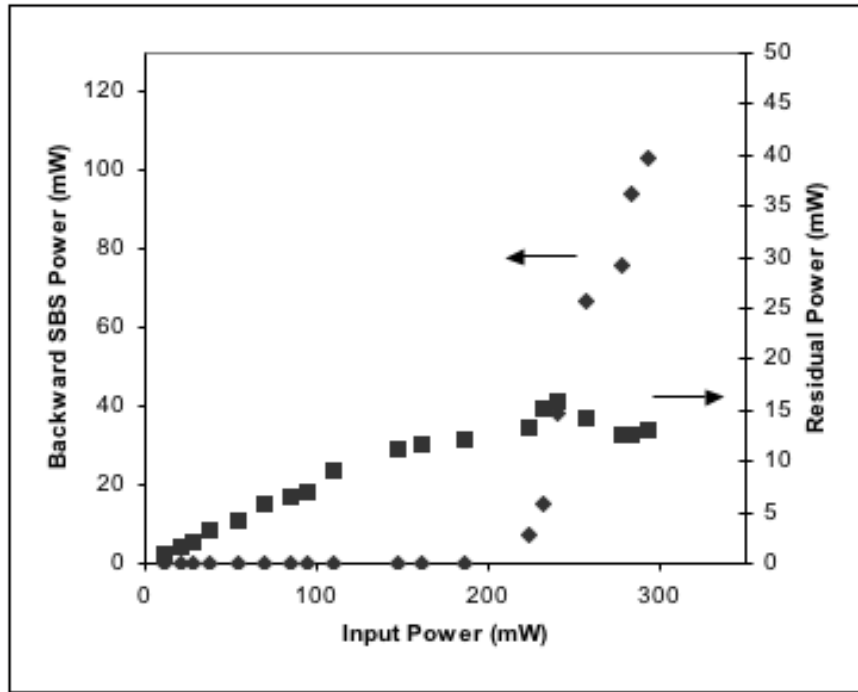
Figure 4.1:   Backwards reflected SBS and residual power vs input power from beam combiner. The fiber was 8.8km of 62.5 μm graded index silica. The conversion efficiency is 38%. Note that slope efficiency is greater than one which was also reported by [7]

100% of the light into the core of both fibers, but this was not observed in practice. The empirical results are consistent with previous work at AFIT [9].

4.2 Off-Axis Beam Combination

The ability to generate a Stokes beam from off-axis side channels was demonstrated. Figure 4.2 shows the input power and the reflected power for a run with peak output power of 989 mW. No Stokes beam was observed at these power levels using either the 62.5 μm or 100μ fiber.

Reoptimization of the fiber amplifier and realignment of the channels allowed a run with peak output of 2.5 Watts from the beam combiner. The input coupling of the 62.5 μm fiber was measured to be 56%. Figure 4.3 shows the input and residual output power of the SBS fiber. A Stokes beam was observed at an input power of 1.581 Watts which is about 4x larger than predicted for the on-axis pumped case. This was confirmed using the Fabry Perot etalon and shown in Figure 4.4. The Stokes beam was seen to flicker in intensity and remained intermittent up to the maximum input power of 2.5W. The traditional roll-off of output power with increasing Stokes power was not observed despite presence of a Stokes beam. The average reflected power measured behind the beam combiner was 50 mW resulting in a conversion efficiency of two percent. The 100 μm fiber did not generate a Stokes beam in the seedless configuration, despite a higher coupling efficiency. This is thought to be due to a much higher SBS threshold.

A second attempt at seedless beam combination was made using the configuration in 3.7 and blocking the output of the center channel. The 62.5 μm fiber was used for this run. Figure 4.2 shows the reflected Stokes power and residual power measured at the end of the SBS fiber as a function of the coupled input power into the SBS fiber. The residual output power does not roll off after the creation of the Stokes beam. Note that the reflected power is only an average. Due to the intermittent nature of the Stokes beam a one minute average was taken and the 1 sigma values calculated by the power meter were used. Observed Stokes beam maximums were usually double,
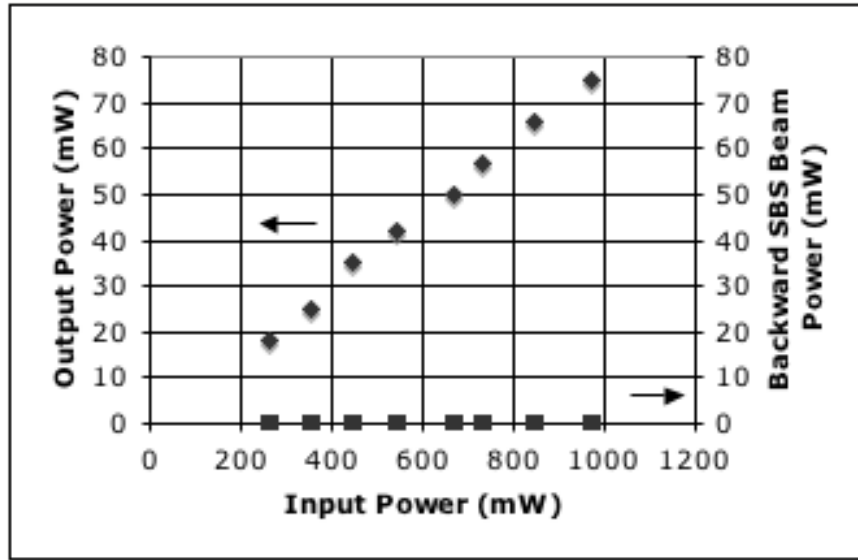
Figure 4.2:   Residual output power throughput of the 62.5 μm
SBS fiber plotted against input power using the configuration in
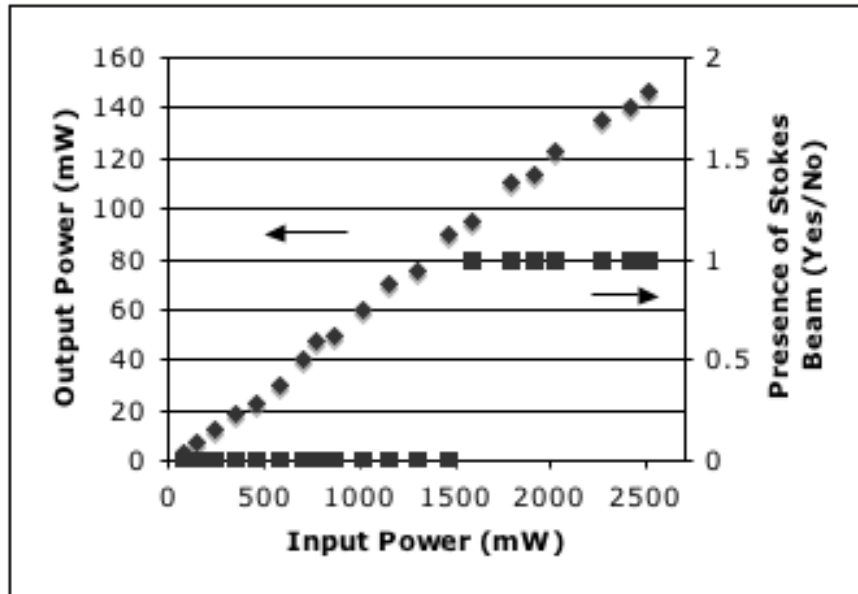Figure 3.4. No reflected Stokes beam was observed.

Figure 4.3:   Residual output power through 62.5 μm SBS fiber
and Yes/No Stokes generation plotted versus input power. 0
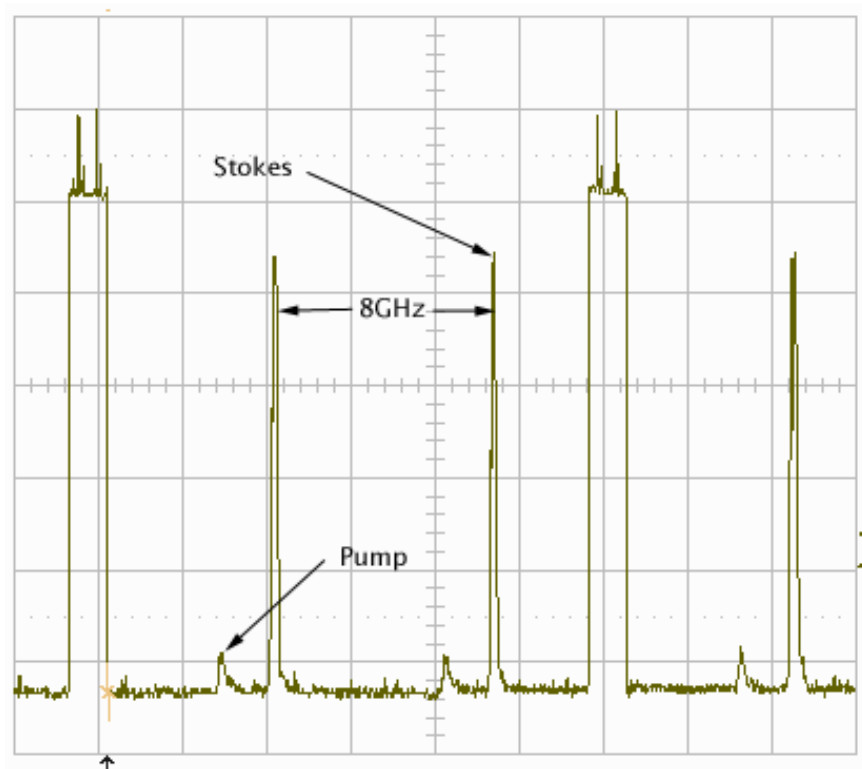represents no Stokes, and 1 represents observed Stokes.

Figure 4.4: Creation of a Stokes beam using four side channels with no center seed. The distance between two Stokes peak is 8 GHz and the spacing between the Stokes and pump peaks is about 16 Ghz.
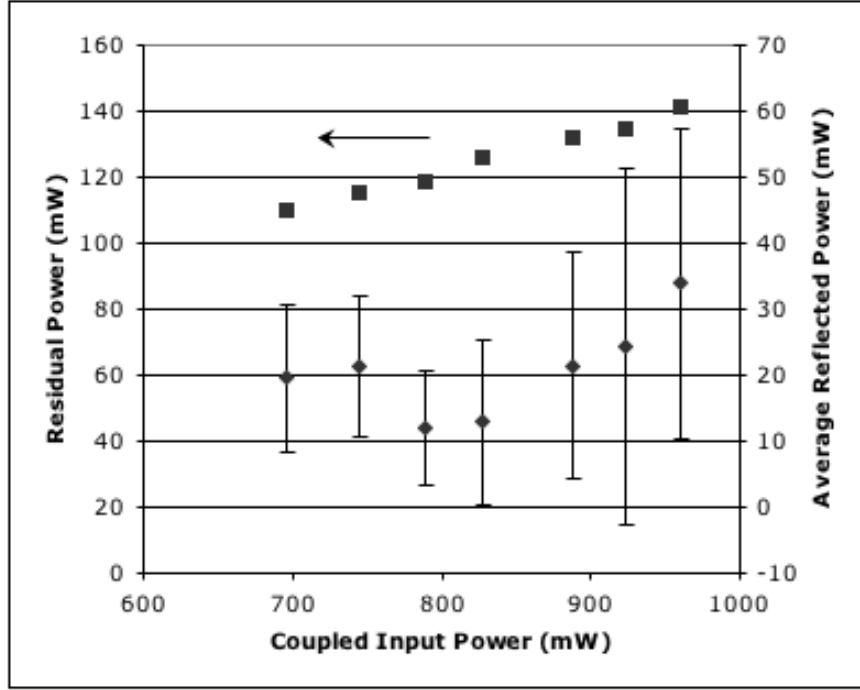
Figure 4.5: Reflected power and throughput power versus input power using the configuration in Figure 3.7 without center channel. Average power was taken over one minute. Error bars are one sigma values given by the power meter. Slope efficiency was calculated to be 11.4%.

and at times four times the average reflected power. The peak average power was 33 mW, and the maximum observed power was about 400 mW. This represents an average conversion efficiency of 3.5% and a peak conversion efficiency of about 41%. The slope efficiency was measured to be 11.4%. The average conversion efficiency compares well to the results obtained above. Due to the intermittent nature of the Stokes beam, a Joule meter was used to take the average energy of the Stokes beam pulses. The energy per pulse, taken as an average over 100 events was 21.6 μJ.

Clearly, the interaction between multiple off-axis pump waves and the created Stokes wave do not fit the current models of SBS production, which assume an on-axis input source that directly stimulates the fundamental mode in the fiber. The large number of modes created and the resultant superposition created by the off-axis inputs does not appear to efficiently couple to the fundamental mode and thus drive

the SBS process in the fiber. Because the experiment had no capacity for feedback of the Stokes beam, SBS must regenerate using random noise. The complicated mode dynamics within the fiber due to the off-axis beams could interrupt this process and result in the observed Stokes fluctuations. The evidence supporting this hypothesis is that unlike when the fundamental mode is stimulated by a pump source, the observed intensity of the Stokes beam created by the off-axis beams continued to fluctuate when power levels were much higher than threshold.

Figure 4.6 is the image taken at the Stokes beam waist in the near field. Figure 4.7 is taken using the same setup, but at the far field using the procedure detailed in Chapter III. Both near and far field images were created using off-axis pump beams with no center seed. Using a Mathematica® nonlinear fit routine, the M^2 value was calculated to be ≤ 1.08, a nearly perfect Gaussian, and demonstrated the cleanup ability of SBS using the GGM concept and a long multimode fiber. Figure 4.8 shows the beam waist as a function of relative position. The exceptional quality of the Stokes beam is an important result and proves that beam cleanup in multimode fibers with multiple off-axis inputs is possible.

After taking measurements of the Stokes beam, the coupling of the side channels was evaluated. Due to the polarization of the input beam and the use of beamsplitters, the balance of power flow through the four channels can be manipulated by adjusting the orientation of a half-wave plate. The ideal balance, along with two notable runs are shown below in Table 4.2. The ideal balance is the channel balance one would get assuming the SBS fiber accepted 100% of the input beams. Since this is not the case due to the imperfect coupling, these runs are presented to show that SBS can be produced using off-axis beams that are each making significant contributions to the total input. The first run in Table 4.2 was the closest match to the ideal case that created a Stokes beam.

The second run, shown in Table 4.2 changed only the channel balance and not the orientation of the beam combiner with respect to the SBS fiber. This was accomplished
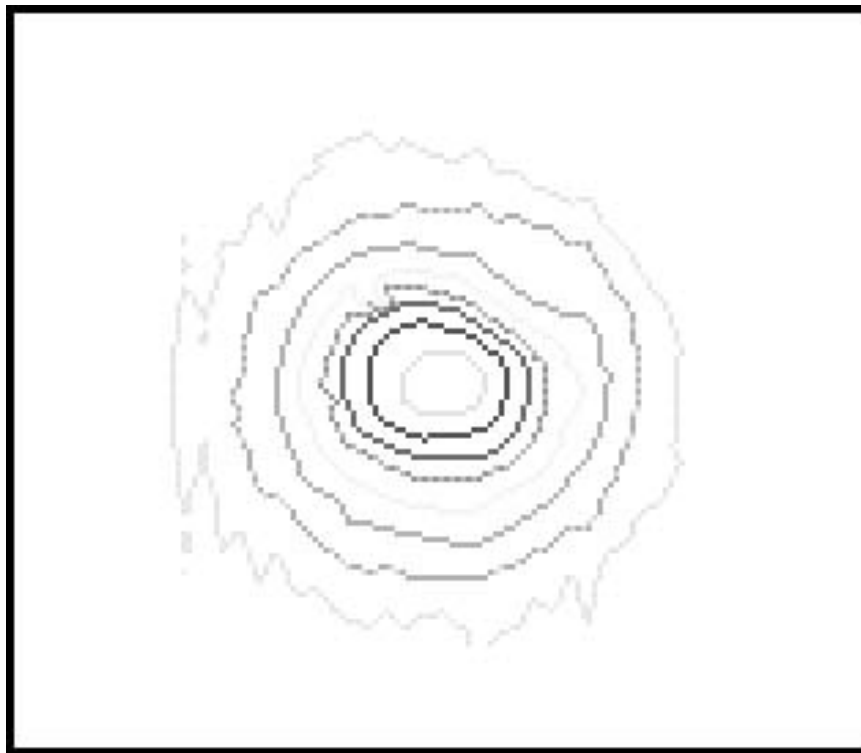
Figure 4.6:   Near field image of Stokes beam created using off-axis beams with no center seed.
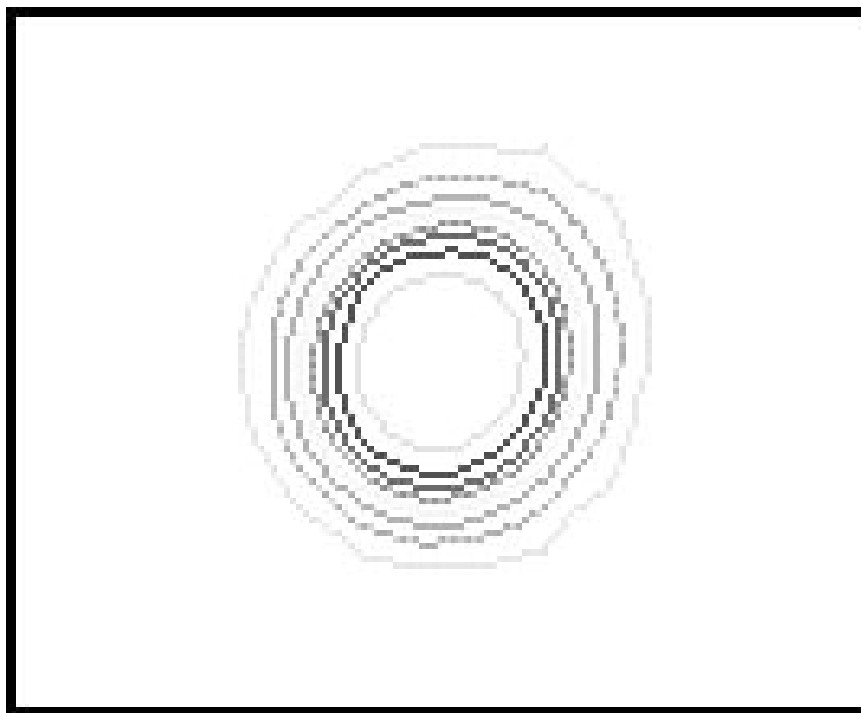

Figure 4.7:   Far field image of Stokes beam created using off-axis beams with no center seed.
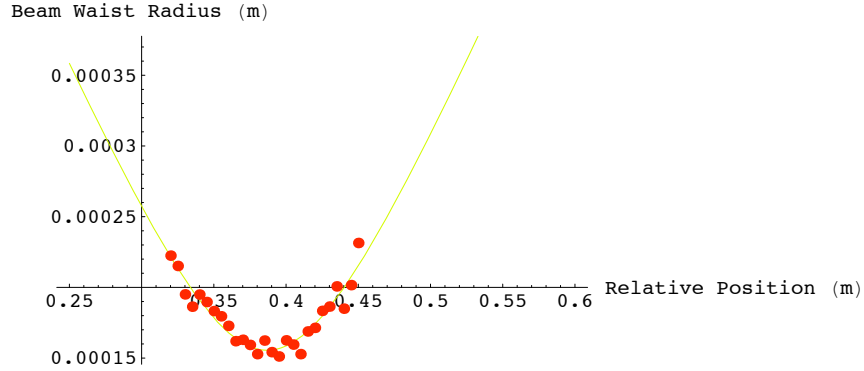
Figure 4.8:   Stokes beam waist versus position using off-axis beams without center seed channel.

by changing the orientation of a half-wave plate. The coupling efficiency of the beam combiner was not calculated due to using the full length of fiber. The total residual throughput for this run was 3.7 mW.

In this case, one channel has been forced to contribute a majority of the input power and will generate SBS, similar to the experiment mentioned in Chapter III where only one side channel was coupled into the SBS fiber. I was not able to determine how much of each channel was contributing to the generation of the Stokes beam due its erratic nature, although in cases where one side channel was contributing a majority of the input power, blocking it effectively killed the Stokes beam.

4.3   Off-Axis Beam Effects on the Center Channel

While the generation of a Stokes beam using only side channels was the most important result of this work, the interplay between the center channel and side channels was also investigated.

Combining a center channel with four side channels proved to be very difficult due to the position of the SBS fiber becoming fixed by the center channel and relying only on the tilt of the beam combiner to couple the side channels. Using only one
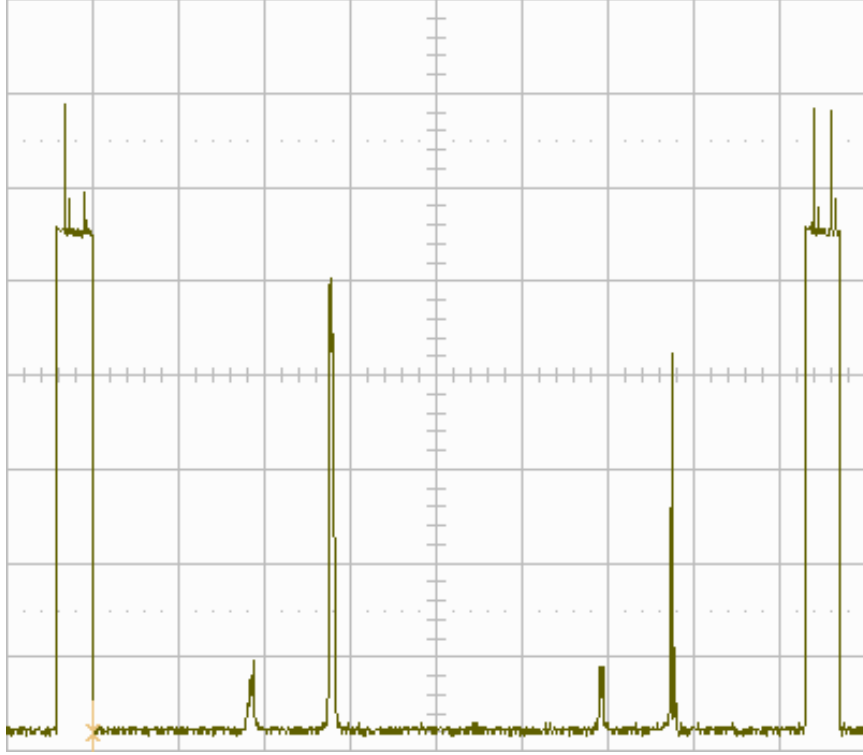
Figure 4.9:   Fabry Perot output using the center seed and one side channel. The Stokes beam intensity was intermittent when the side channel was on and steady when it was off. Note the difference in height of the two Stokes peaks.

side channel and the center seed, I was able to qualitatively demonstrate that the intermittent Stokes beam is a consequence of the side channel coupling. Using only the center channel, a steady Stokes beam was observed at the pickoff in Figure 3.7.

When the side channel was turned on, the Stokes signal at the pickoff became intermittent and fluctuated wildly as if it was at threshold. It would appear that the side channel disrupts the generation of the Stokes beam due to the large number of modes being produced in the SBS fiber and the poor coupling to the fundamental mode by the superposition.

4.4   Chopped Input Beam Combination

After observing the intermittent nature of the Stokes beam output using a continuous input source, a beam chopper was used to investigate the effects of a tempo-

rally modulated input. The chopped beam approximated a square wave input versus a continuous signal. A beam chopper with a pulse rate of 130 Hz and a pulse duration of 1.83 ms was used. The average energy per pulse of the Stokes beam taken over 200 events was 9.3 μJ. The power per pulse, assuming a 1.83 ms pulse width was approximately 5 mW. This result is much lower than the average power when using CW input. The average power throughput at the end of the SBS fiber dropped from 75$\pm$mW to 18.5$\pm$ mW with the chopper in place. At an input power of 1.55 W, this represents an efficiency of 0.32%. The deleterious effect of the beam chopper was evident in the reduced reflected power, but had no observable effect on the stability of the Stokes beam.

Table 4.1:   One meter side channel coupling test with 45% total coupling efficiency

Channel	Ideal Contribution	Contribution	Percent Contribution
1	12.5%	5 mW	3.9%
2	12.5%	42 mW	32.8%
3	25%	58 mW	45.3%
4	25%	23 mW	17.9%

Table 4.2:   8 km side channel coupling test

Channel	Power Contribution	Percent Contribution
1	0.1 mW	2.7%
2	0.4 mW	10.8%
3	3.0 mW	81%
4	0.1 mW	2.7%

V. Summary and Justification for Future Work

5.1 Summary

IN this thesis I have quantitatively demonstrated the ability to generate a single Stokes beam from four off-axis beams using a fiber array beam combiner and a long multimode fiber. The resulting output from the combination the off-axis beams is a single, near perfect Gaussian beam with an M² value of ≤1.08. The GGM and beam combiner concept allowed efficient combination of the input beams with coupling efficiencies of 61% for a 62.5μm core fiber and 89% for a 100 μm core fiber. The GGM provided a way for each input beam to contribute a significant percentage of the individual power totals to the core of the SBS fiber. While the beam quality generated by SBS was excellent, the conversion efficiency was quite low. The average conversion efficiency was about 3.5% with a slope efficiency of 11.4%. However, due to the fluctuation of the Stokes beam, the peak conversion efficiency was closer to 42%. When the input beam was chopped with a period of 130 Hz, a Stokes beam was still created, but the average power dropped considerably to 5 mW, representing a conversion efficiency of just 0.32%. The creation of the Stokes beam using off-axis beams requires much higher input powers, on the order of 4x the threshold in the on-axis input case. It is clear that there is difficulty in coupling the multimode pump wave created by the input geometry to the fundamental mode and efficiently extracting power from the created Stokes wave.

Perhaps the most surprising result of this work was that a cw input divided among four channels and focused into a optical fiber would generate a Stokes beam that oscillates in intensity with no determinable period. I qualitatively demonstrated that these fluctuations in Stokes intensity are caused by the presence of off-axis beams. The Stokes beam intensity was constant in intensity when only the center on-axis seed beam was present. The addition of a single side channel creates significant temporal intensity oscillations in the Stokes beam. These oscillations are erratic with no determinable period. Rather than a partial dip in Stokes intensity, the Stokes

beam appeared to completely extinguish between observed maximums, as if coupled intensity was near threshold.

5.2 Justification for Future Work

The combination of multiple low power lasers into a single high quality beam has been an important defense research topic in the last 25 years. This thesis represents an evolutionary increase in the capability to combine multiple laser beams. Since the generation of a Stokes beam using SBS in an optical fiber was demonstrated in 1972, researchers have successfully increased both the quantity of beams combined and the quality of the reflected Stokes beam. While reflected beam power levels remain low, the combined beam quality is excellent. There is clear indication that the underlying physics is sound and the engineering problems solvable to allow for larger arrays and higher powers.

One of the main concerns for achieving higher power is the limitations of the fibers themselves. Smaller fibers require lower thresholds for generating SBS, but also bring with them a reduction in core size, which limits the number of beams one can combine. As shown in this thesis, even small fibers have quite large SBS thresholds. These thresholds are predicted to scale with increasing core size. Second, since the SBS fibers themselves have losses, high input powers can easily destroy the SBS fiber, especially near the input since a majority of the SBS conversion occurs in that region. Third, SBS requires a narrow linewidth source. With current technology, such sources are only available in select wavelengths, many of which are not ideal for missions that deny or degrade enemy capabilities.

The GGM concept proved to be a very good method of physically combining many beams. The two main issues with the GGM are producing a collimated output and keeping each beam parallel to the front facet of the combining lens. GRIN lenses proved effective at providing a collimated output, but the GGM requires improved machining and more precise alignment than hand-assembly can provide. Larger GGMs

may cause difficulty servicing individual elements and extracting the Stokes beam due to the close-packed hexagonal configuration.

Future work will be able to improve upon the beam combiner concept by taking advantage of higher power sources and more exotic fibers that will allow higher coupling efficiency and lower SBS thresholds. Using current technology, one possibility would be to create a fiber Brillouin laser that is end pumped by the beam combiner. The configuration is shown in Figure 5.1.

This setup combines the ability of off-axis beams to create a Stokes beam within a fiber, with the concept of a Brillouin fiber laser. Such a laser could use many pump sources and efficiently scale up in power. One could also pump from both ends or employ a ring cavity. The advantage of using an off-axis pumped fiber Brillouin laser is that the threshold power required for SBS should be considerably reduced from what was observed using only off-axis beams because feedback is now provided by the cavity. The factor of 21 in Equation 2.19 can be reduced to between 0.1 and 1 depending on the coupling losses. [4, p. 280]. The feedback in the cavity would also provide enhanced coupling to the fundamental mode by the off-axis pump beams.
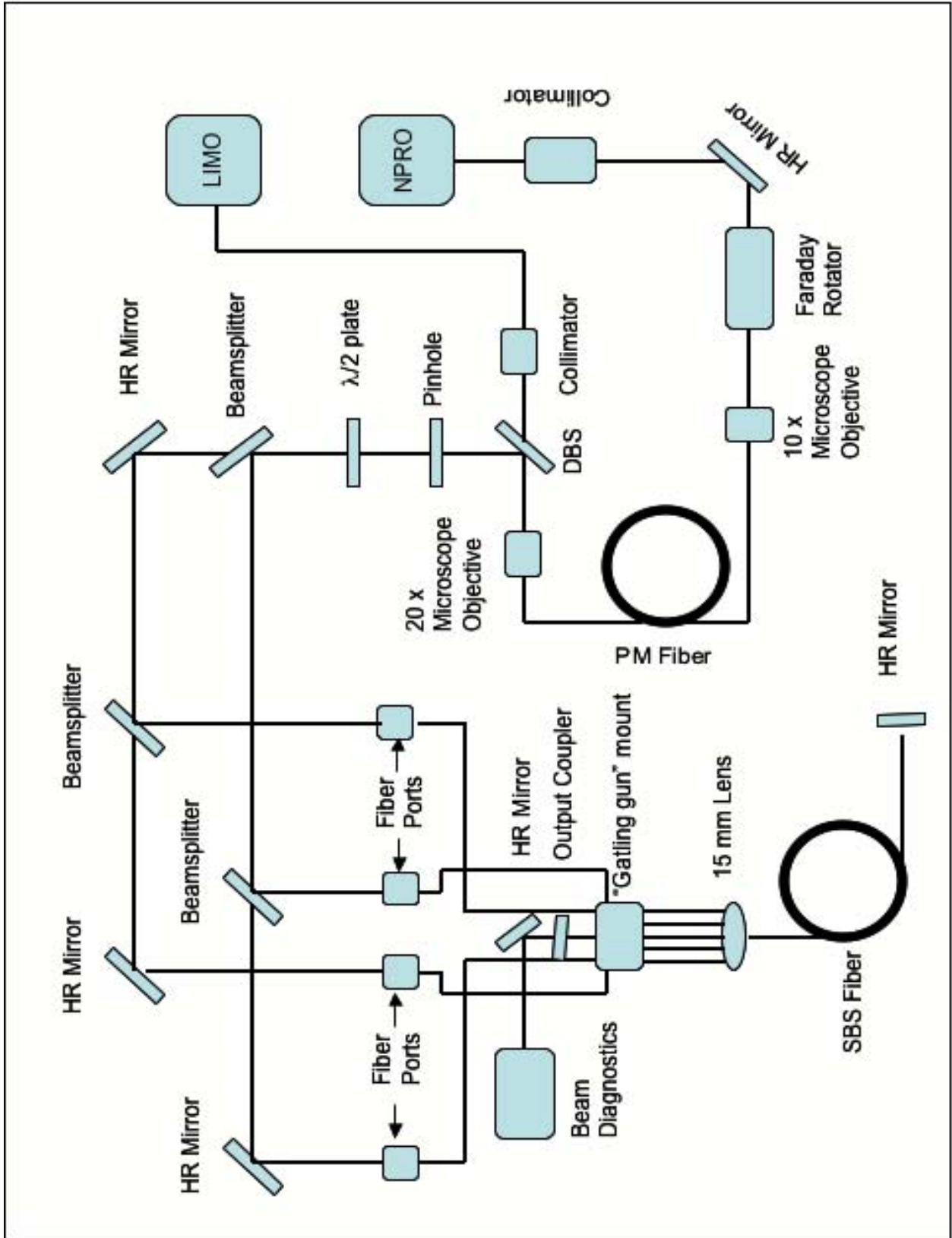
Figure 5.1:   Concept for an off-axis end-fed Brillouin laser us-
ing existing pump source with the addition of a resonator cavity.

Bibliography

1. "Encyclopedia of Laser Physics and Technology". URL `http://www.rp-photonics.com/fibers.html`.

2. "Encyclopedia of Laser Physics and Technology". URL `http://www.rp-photonics.com/beamquality.html`.

3. "Single-Beam Optical Gradient Trap". URL `www.sia.uq.edu.au/physics/light/tweezers.html`.

4. Agrawal, G.P. *Nonlinear Fiber Optics*. Academic Press, Inc., 1989.

5. Aoki, Yahuriro and Kazuhito Tajima. "Simulated Brillouin scattering in a long single-mode fiber excited with a multimode pump laser". *Journal of the Optical Society of America B*, 5(2):358–363, February 1988.

6. Boyd, R.W. *Nonlinear Optics*. Academic Press, 2003.

7. Brusselbach, Hans. "Beam cleanup using stimulated Brillouin scattering in multimode fibers". *Conference on Lasers and Electo-Optics*, 424–426. 1993.

8. Grime, Brent W. *Multiple Channel Laser Beam Combination and Phasing Using Stimulated Brillouin Scattering In Optical Fibers*. Ph.D. thesis, Air Force Institute of Technology, 2005.

9. Grime, Brent W., Nathan B. Terry, Timothy H. Russell, and Won B. Roh. "Efficient Mulitple-Beam Combining in Stimulated Brillouin Scattering Fiber Beam Combiner". *Beam-8*. 2001.

10. Hecht, Eugene. *Optics, 4th Edition*. Addison Wesley, 2002.

11. Ippen, E.P. and R.H. Stolen. "Stimulated Brillouin scattering in optical fibers". *Applied Physics Letters*, 21(11):539–540, December 1972.

12. Okoshi, Takanori. *Optical Fibers*. Academic Press, 1982.

13. Rogers, Blake C. *Laser Beam Combining and Cleanup via Stimulated Brillouin Scattering in Multimode Optical Fibers*. Master's thesis, Air Force Institute of Technology, 1999.

14. Rogers, Blake C., Timothy H. Russell, and Won B. Roh. "Laser beam combining and cleanup by stimulated brillouin scattering in a multimode optical fiber". *Optics Letters*, 24(16):1124–1126, August 1999.

15. Russell, Timothy H. *Laser Intensity Scaling Through Stimulated Scattering in Optical Fibers*. Ph.D. thesis, Air Force Institute of Technology, 2003.

16. Russell, Timothy H. and Won B. Roh. "Incoherent beam combining using stimulated Brillouin scattering in multimode fibers". *Optics Express*, 8(2):246–254, February 2001.

17. Russell, Timothy H. and Won B. Roh. "Threshold of second-order stimulated Brillouin scattering in optical fiber". *Journal of the Optical Society of America B*, 19(10):2341–2345, October 2002.

18. Sjoberg, Mats, Manuel Quiroga-Teixeiro, Sheila Galt, and Sverker Hård. "Dependence of stimulated Brillouin scattering in mulitmode fiber on beam quality,pulse duration, and coherence length". *Journal of the Optical Society of America B*, 20(3):434–442, March 2003.

19. Sternklar, Shmuel, Doron Chomsky, Steven Jackal, and Arie Zigler. "Misalignment sensitivity of beam combining by stimulated Brillouin scattering". *Optics Letters*, 15(9):469–470, May 1990.

20. Wallace, John. "Life Before M2". *Laser Focus World*, November 2005.

21. Zeldovich, Y.B., N.F. Pilipetsky, and V.V. Shkunov. *Principles of Phase Conjugation.* Springer, 1985.

REPORT DOCUMENTATION PAGE

Form Approved
OMB No. 0704-0188

Public reporting burden for this collection of information is estimated to average 1 hour per response, including the time for reviewing instructions, searching data sources, gathering and maintaining the data needed, and completing and reviewing the collection of information. Send comments regarding this burden estimate or any other aspect of this collection of information, including suggestions for reducing this burden to Washington Headquarters Service, Directorate for Information Operations and Reports, 1215 Jefferson Davis Highway, Suite 1204, Arlington, VA 22202-4302, and to the Office of Management and Budget, Paperwork Reduction Project (0704-0188) Washington, DC 20503.
PLEASE DO NOT RETURN YOUR FORM TO THE ABOVE ADDRESS.

1. REPORT DATE *(DD-MM-YYYY)* 16-03-2006	2. REPORT TYPE Master's Thesis	3. DATES COVERED *(From - To)* Jul 2005 - Mar 2006

4. TITLE AND SUBTITLE
Passive Multiple Beam Combination in Optical Fibers via Stimulated Brillouin Scattering

5a. CONTRACT NUMBER

5b. GRANT NUMBER

5c. PROGRAM ELEMENT NUMBER

6. AUTHOR(S)
Brown, Kirk C., Capt, USAF

5d. PROJECT NUMBER
NAFRL056209093

5e. TASK NUMBER

5f. WORK UNIT NUMBER

7. PERFORMING ORGANIZATION NAME(S) AND ADDRESS(ES)
Air Force Institute of Technology
Graduate School of Engineering and Management (AFIT/EN)
2950 Hobson Way
WPAFB, OH 45433-7765

8. PERFORMING ORGANIZATION REPORT NUMBER
AFIT/GAP/ENP/06-01

9. SPONSORING/MONITORING AGENCY NAME(S) AND ADDRESS(ES)
AFRL/DELO
ATTN: Rick Berdine
3550 Aberdeen Ave SE
Kirtland AFB, NM 87117-5776
505-853-4342

10. SPONSOR/MONITOR'S ACRONYM(S)

11. SPONSORING/MONITORING AGENCY REPORT NUMBER

12. DISTRIBUTION AVAILABILITY STATEMENT
APPROVED FOR PUBLIC RELEASE; DISTRIBUTION UNLIMITED

13. SUPPLEMENTARY NOTES

14. ABSTRACT
The goal of this research was to demonstrate the feasibility of passively combining multiple laser beams using Stimulated Brillouin Scattering (SBS) in a long multimode optical fiber. This method of combination employed a "Gatling gun" fiber array that allowed several collimated beams to be focused by a lens into an optical fiber. The ability to combine four single-mode off-axis input beams using a fiber array and a long multimode optical fiber was demonstrated. The Stokes beam generated by the four off-axis input beams was found to be near Gaussian with an M^2 value of < 1.08. The maximum average reflected power was approximately 50 mW with a conversion efficiency of 3.5% and a slope efficiency of 11.4%. The deleterious effects of the addition of an off-axis side channel was demonstrated. The addition of just one side channel caused the Stokes beam to become erratic and fluctuate in intensity with no discernible period.

15. SUBJECT TERMS
Stimulated Brillouin Scattering, Beam Combination, Beam Cleanup, Fiber Lasers, Stokes Beam

16. SECURITY CLASSIFICATION OF:			17. LIMITATION OF ABSTRACT UU	18. NUMBER OF PAGES 64	19a. NAME OF RESPONSIBLE PERSON Timothy H. Russell, AFIT/ENP
a. REPORT U	b. ABSTRACT U	c. THIS PAGE U			19b. TELEPONE NUMBER *(Include area code)* 937-255-6565, email: timothy.russell@afit.edu

Standard Form 298 (Rev. 8-98)
Prescribed by ANSI-Std Z39-18